POLITECNICO

MILANO 1863

SCUOLA DI INGEGNERIA INDUSTRIALE
E DELL'INFORMAZIONE

Ion Generation in the Emitter Region of Electrohydrodynamic Thrusters

TESI DI LAUREA MAGISTRALE IN
AERONAUTICAL ENGINEERING - INGEGNERIA AERONAUTICA

Author: **Giuseppe Caliò**

Student ID: 991786
Advisor: Prof. Paolo Francesco Barbante
Co-advisors: Carlo De Falco, Lorenzo Valdettaro
Academic Year: 2022-2023

Why should we try to be our best
When we can just get by and still gain?
Jonathan Larson

Sommario

Lo sviluppo di propulsori elettroidrodinamici, comunemente detti a vento ionico, potrebbe rappresentare una svolta nella propulsione di una nuova generazione di dirigibili e aeromobili. Questi propulsori sono caratterizzati da unità prive di parti meccaniche mobili e perciò presentano tempi operativi molto lunghi, richiedono poca manutenzione e sono estremamente sostenibili dal punto di vista delle emissioni in atmosfera. Il design ottimale di questi sistemi richiede un considerevole sforzo nella ricerca fondamentale e applicata. Uno strumento di simulazione che sia efficiente e accurato rappresenterebbe un valido supporto per i progettisti. Questa tesi, estendendo il lavoro svolto da [36], mira a proporre un modello fluido autoconsistente per simulare la corrente di plasma non termico che si genera tra i due elettrodi, gettando le basi per sviluppi futuri in questo campo. L'implementazione numerica del modello è stata prodotta attraverso GNU OCTAVE; il metodo agli elementi finiti è stato usato per la discretiazzione spaziale, mentre uno schema di *splitting* con dimensione degli intervalli temporali adattivo è stato usato per l'integrazione nel tempo. La scarica in regime di corrente continua a pressione atmosferica è ampiamente documentata in letteratura, in particolare con Argon come gas di alimentazione. Per questo motivo le simulazioni di questa tesi sono state svolte in Argon. Sono stati condotti alcuni esperimenti numerici e i risultati sono stati in seguito analizzati e alcune considerazioni esposte.

Parole Chiave: scarica a pressione atmosferica, modello fluido, propulsori ionici, plasma non termico.

Abstract

Electrohydrodynamic (EHD) propulsive systems could represent a cross-cutting technology in driving a new generation of airships and aircraft. This kind of thrusters is characterised by propulsive units without moving mechanical parts, therefore having extremely long operation times, low maintenance and very low pollution. The optimal design of such systems requires a lot of effort both in fundamental and applied research. An efficient and accurate simulation tool could help in the design and optimization process. This thesis, extending the work done by [36], aims at proposing a self-consistent 1D fluid model to properly simulate the non- thermal plasma flow arising between the electrodes, providing an initial a first theoretical and mathematical framework for future developments in the field. Its numerical implementation is performed through GNU OCTAVE; it is based on a finite element method for the spatial discretization and a splitting scheme with adaptive stepsize solver for time integration. The Direct-Current (DC) discharge at atmospheric pressure is widely documented in literature, especially with Argon as feed gas, providing results for preliminary verification of the model; for this reason Argon is the gas used in all the simulations. Numerical experiments have been performed; then the results have been analysed and some considerations drawn.

Keywords: atmospheric pressure discharges, fluid model, EHD thrusters, non-thermal plasma.

Contents

1 | Introduction

1.1. Review of EHD propulsion

Non-thermal or low temperature plasmas (LTP) are essentially plasmas in which there is no thermodynamic equilibrium among the components of the medium. The interest in this kind of plasmas has been growing in the last years because of the considerable variety of possible applications: from surface treatments of different materials to production of integrated circuits, to electrohydrodynamic (EHD) thrusters for atmospheric propulsion in the aeronautical field. A non-exhaustive brief description of the possible applications is depicted in [36].

Study of non-thermal plasma for atmospheric propulsion is a subject of ongoing investigations. In recent years, a lot of experimental studies have been carried out showing the potential of this technology. For example [25] studied the electrohydrodynamic thrust generated by wire–cylinder electrodes under high Direct-Current (DC) voltage, providing comparisons with theoretical predictions based on a simple 1D model, previous measurements and investigating the effect of the geometry and materials of the emitter. [3] focused on a parametric study of the performance of such EHD thruster as a function of the electrode geometry, with particular attention toward the collector. Different collectors shaped as NACA airfoils were tested through the experimental apparatus shown in Figure 1.1, NACA 0010 turning out to be the most interesting one for further studies.
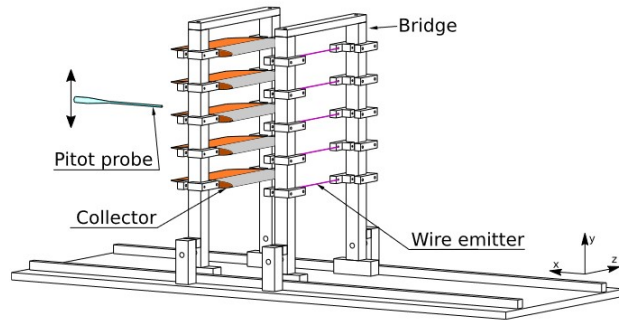

Figure 1.1: Experimental setup of [3]

A proof of concept for EHD propulsion is offered, instead, by [39] in which a steady-level flight for a short of time has been achieved with a fixed-wing airplane (Figure 1.2).

Figure 1.2: Proof of concept built at MIT, from [39]

From the numerical point of view a lot of work has been done for the simulation of micro-scale corona discharges in the noble gas Helium, with different purposes like surface treatments of materials or thermal cooling for semiconductor devices or even electrothermal microthrusters [17]. The non-equilibrium nature of this kind of plasma was already observed in [17], where the electron temperatures were found to be of tens of electronvolt while the gas temperatures only hundreds of Kelvin. The methodologies adopted for the investigation of the discharges in Helium have been repurposed for studying the noble gas Argon in the most recent researches.

[2] investigated the transition from the α regime (low current density) to the γ regime (high current density) in Argon. A self consistent fluid model was proposed to simulate the atmospheric RF (radio frequency) discharge. The model consists of one continuity equation for each component of the plasma, the electron energy equation and the Poisson equation for the self-consistent electric field. The simulation is done in a one dimensional grid representing a gap of 2 mm, therefore 2D and 3D effects are neglected. The authors assume the neutral gas and the heavy ion temperature to be constant and equal, meaning that the energy gain/loss of the gas/ions is negligible; the electrons equation instead is simplified accounting for energy exchange by averaged loss and gain terms coming from the collisions with other plasma population. Different treatments of the energy equations is offered by ref. [10], that in turn is based on the ref. [17]. In these works the physical model is based on a two-dimensional, self-consistent, multi-species, two-temperature, fluid description of the plasma. The temperatures are those of the electrons and the gas/ions. The high pressure (where "high" stand for tens or hundreds of Torr) increases the collisionality that in turn lead to dissipate the input power in gas heating: therefore the gas temperature is not constant. The implication is that also some reaction rates will change because of the dependency on the gas temperature, leading to different production terms in the continuity equation. Nevertheless, this last model presents another peculiarity:

the neutral argon is treated as "background gas" and its density computed not from a PDE but leveraging on the ideal gas law. In general, both air and argon at atmospheric condition could be safely treated as ideal gas; however the computational savings are not that much.

With the aim of providing a basis for future research effort, a complete fluid approach as in ref. [2] will be pursued, with the difference that the Local Field Approximation (LFA) will be restored as explained in chapter 2. The plasma chemistry in the above cited works appears also to be different, with ref. [10] having a richer reactions system than ref. [2].The choice for this thesis is in favour of the simpler chemical model [2], since it has been taken as a starting point the results of [36]. Nevertheless, it will be shown as the developed solver can quickly be set up with different chemical reactors. From the numerical point of view the difficulties come from the stiffness of the equations, due to the different time scales that the chemical reactions show. However, chemistry is not the unique contribution to stiffness. Indeed, there is a huge difference also in the time scales of the others involved physical phenomena, namely diffusion and drift, as discussed in chapter 3; furthermore the system is highly non linear because of the couplings among the continuity equations themselves, that come from the chemical source term, and among the transport terms with the self-consistent potential. In particular the dominant transport phenomena appears to be the drift one, increasing the non linearity. In other words, the addressed problem is mathematically tough, even when the physics is simplified. The numerical model of [[2],[10]] is based on finite volume discretization and in order to overcome the mentioned difficulties the flux is discretized with a scheme equivalent to the Scharfetter-Gummel exponential one; they proposed also a semi-implicit time integration for stability reasons and to keep a relatively high simulation time step. However in this work the Finite Element Method (FEM) will be pursued, still employing the Scharfetter-Gummel exponential scheme for the flux discretization.

The model adopted in this thesis is not the unique possibility to simulate the ionic wind in EHD thrusters. More advanced models are available in literature, even if not yet tested for the specific field of interest here. In order to collocate properly this thesis in the IPROP project it is useful to devote a brief description of them.

As already mentioned, the peculiar feature of LTPs is their non-equilibrium nature, that will cause a more or less significant departure of the electron distribution function (EDF) from being Maxwellian. [16] presents an overview of the last advances in electron kinetic of LTPs in different areas. It is pointed out how, in general, a fluid approach can be adopted because of the high pressure, but it is in general wrong to assume the local equilibrium of the electrons. Indeed, the high electric field and the reduced dimensions encountered contribute to a departure from local kinetics.

The work done in a close research field, namely plasma thruster based on the Hall effect [20], suggests the possibility to adopt an hybrid model, in which the electrons are described by the Boltzmann equation and ions and neutrals are still governed by fluid equations: this approach would be a novelty in the field of EHD thruster. Another approach is suggested by ref. [19]. The authors propose a new moment based method that is potentially more accurate than the fluid approach, but still less than the hybrid one. It seems valid from a theoretical point of view and the comparison with Direct Simulation Monte Carlo (DSMC) shows its potential in capturing non Maxwellian EDF in LTPs. These observations should clarify the existence of other possibilities on which future studies could be devoted.

The reason to choose the fluid model in this thesis is related to the choice of starting from scratch to develop a solver in which more and more physical aspect are progressively included, in order to have a complete awareness of their effects. This path will allow in future to consider only those physical features that could be potentially relevant for the design of EHD thrusters. From an engineering point of view, the complexity of the model, that comes together with computational costs, should be justified by a quantitative analysis on how much the accuracy could be improved with respect the most simple one. In this perspective, starting from the simplest existing approach, namely the fluid one, appears interesting. It is possible to reason about what are the limits and the missing plasma flow features and, eventually go for progressive advancements. At each step of this process one should compare the improvement in the accuracy versus the additional computational effort.

1.2.   Physics of EHD propulsion

The physical phenomena that lead to the generation of propulsive forces in EHD thrusters are quite well understood and are going to be explained in the following.

Ions are generated in the ambient gas by a corona, which is a weakly luminous discharge characterized by a spatial non-uniformity. Indeed it is possible to distinguish a *corona region* or *ionization layer*, located near one electrode, in which the plasma generation, the high electric field and the source of light are all located [12]. The confinement of the plasma generation around one active electrode is obtained thanks to its geometry: for example a thin wire can sustain a strong electric field in its proximity [6]. Beyond the ionization layer, there is the so called *drift region*, in which the generated ions can travel and where further ion generation is not possible because of the low electric field.

There are two kind of corona, namely negative corona and positive one, depending on
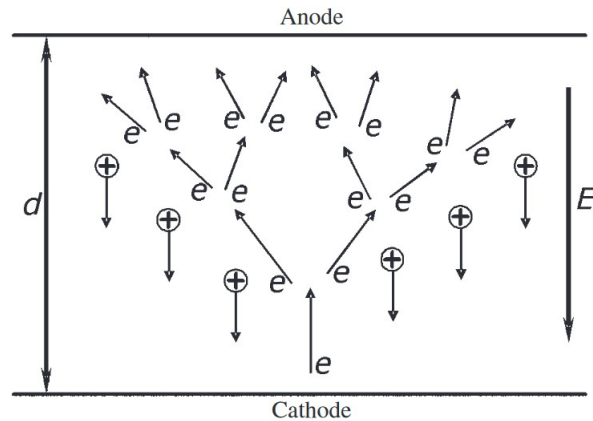
Figure 1.3: Townsend avalanche [12]

the fact if the strong electric field is located in the region of the cathode or of the anode, respectively. In both cases the discharge is characterized by a chain of ionization events, located near the active electrode.

The negative corona follows a breakdown mechanism similar to the Townsend avalanche [12]. This mechanism was firstly discovered by Townsend in 1897. He observed an exponential increase in the current, due to the energized electrons that leaving the cathode caused ionization of the gas molecule by collisions[18]. Therefore, differently from a corona, the discharge is quite uniform in the gap and there are no drift zones (Fig.1.3).

The mechanism of positive corona is a little bit different and in this thesis, the attention will be focused on this kind of discharge, considering a configuration with one grounded electrode, that serves as cathode and a high voltage electrode that serves as anode, around which the active corona volume is.

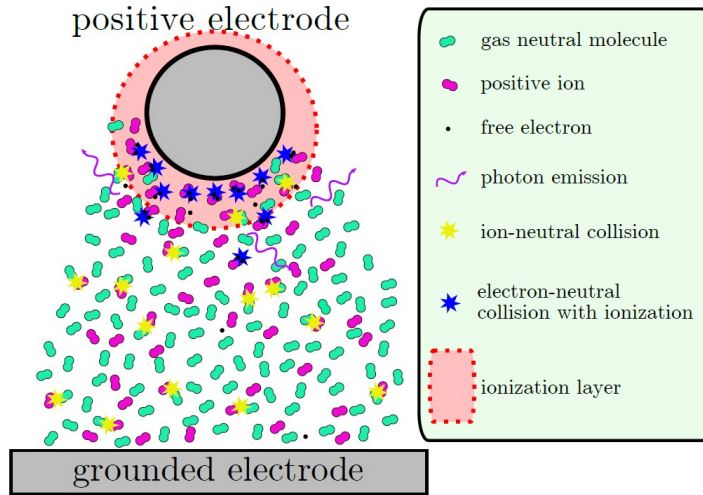A qualitative representation of such situation is depicted in Figure 1.4.

Figure 1.4: Qualitative depiction of positive corona discharge in gas [6]

The corona discharge that generates the positive ions is indeed induced by the application of a high electric potential between these two electrodes. Inside the corona region, near the anode, the electric field accelerates electrons that create a cascade of ionization events mainly by electron-neutral gas collision [39]. The corona discharge is in a self-sustained and stable regime when the applied electric field is high enough to overcome the local dielectric strength of air and low enough to avoid an electric arc between the electrodes. The electrons are quickly captured by the positive electrode, leaving behind a wake of positive ions [11], that are accelerated from the plasma region by the Coulomb force due to the applied electric field, and drifts in the low electric field portion of the gap. These accelerated ions transfer momentum to neutral gas molecules by collision; the resulting ionic wind generates a thrust force in the direction opposite to ion flow.

In this brief description of the corona discharge is hidden a basic explanation about the non-equilibrium nature of the generated plasma. The electrostatic energy is primarily absorbed by electrons, which are accelerated and collide with the background neutral gas, sustaining the above depicted mechanisms. Therefore the gas stream is weakly heated and remains close to ambient pressure. Following this point, one can imagine to describe the physics of the discharge considering a condition in which at least particles of the same species are locally in thermal equilibrium. From a modeling point of view, this hypothesis justifies the adoption of a two-temperature fluid-like model, in which the electrons have their own temperature T_e, while ions and neutral gas are at T_i. The energy transfer among the ionized gas is described by two energy equations. This assumption is fundamental in the present work, that is based on developing a fluid-like approach. However, it presents severe limitations that should be pointed out from the beginning: the high-collisionality

due to the high pressure is not enough to justify local kinetics [16]. In fact, it can happen that the energy relaxation length becomes comparable to the ionization region size making non local effects relevant [16], [35] and in this case, the electron energy distribution function (EEDF) would depart from the Maxwellian condition. However, this point will be discussed further in chapter 2. This condition would require more advanced models that are discussed in the section devoted to possible future developments (chapter 6). However, with a fluid model some of the mentioned features of the discharge can be captured: the ions generation in the anode emitter region, their drift towards the cathode and the confinement of a ionization layer close to the emitter.

1.3. Structure and scope of the thesis

This thesis is born in the research framework of the Ionic PROPulsion (IPROP) project, that aims at engineering a flying airships driven by an EHD thruster. In the field of EHD propulsion a numerical model, able to match experimental results and to make predictions driving the design choices, is still lacking. Indeed, a simulation tool would help engineers in finding the optimal design parameters to improve performance for each different application and condition. The scope of this work is to provide a suitable mathematical model able to catch some physical features of ionic thrusters, and more precisely on the plasma flow arising in the discharge. The adoption of a fluid model like the one of [2] in ionic propulsion represent a novelty in the field, since the most of the research efforts up to now have been of experimental nature. Nevertheless, it cannot be seen as the final output of IPROP projects, that aims at building more advanced models, as the ones mentioned in the literature review.

Despite its relative simplicity, the fluid model allows to deal with some difficulties (very stiff equations, chemical non equilibrium, etc.) that help in gaining the required know-how for future studies. The thesis is structured as follows: in chapter 2 a theoretical description of the physical and mathematical model is presented together with a discussion on the limit of validity of the hypotheses adopted; in chapter 3 some mathematical feature of the equations and the numerical strategies for solving them are depicted; in chapter 4 test for the solver validation are shown; in chapter 5 the results of the simulations performed are reported and commented. Finally chapter 6 presents the conclusions and hints for further developments.

2 | Physical Model

This chapter presents the equations that are going to be solved, together with the assumptions and simplifications adopted. It has been preferred to start from the general Boltzmann equation to show step by step all the hypotheses required to end up with a multiple fluid model. This way of proceeding has been thought to make as clear as possible the limit of validity of the model, that is quite relevant in perspective of future research.

In particular, the drift-diffusion approximation will be introduced to get rid of the momentum equation and the chemical reactions are accounted for by providing a source term in the continuity equation of each species. Models for transport and reaction rates coefficient are introduced and finally the self-consistent electric field is computed through the Poisson equation.

2.1. Plasma Fluid model

A general way to derive fluid equations for a plasma is starting from the Boltzmann equation, that describes the time evolution of the distribution function in phase space. Given a partially ionized plasma composed of N species the Boltzmann equation for each of them reads:

$$\frac{\partial f_k}{\partial t} + \mathbf{v} \cdot \nabla_{\mathbf{x}} f_k + \frac{\mathbf{F}_k}{m_k} \cdot \nabla_{\mathbf{v}} f_k = \left. \frac{\partial f_k}{\partial t} \right|_c \tag{2.1}$$

where f_k is the distribution function of the kth species, $\mathbf{F}_k = q_k \left(\mathbf{E} + \mathbf{v} \times \mathbf{B} \right)$ the Lorentz force and

$$\left. \frac{\partial f_k}{\partial t} \right|_c = C_k$$

the collision term, expressing the time variation of f_k by short range interactions among species. For each species their charge is defined as

$$q_k = e z_k$$

with

$$z_k = \pm|z_k|$$

the valence number of the kth species multiplied by the sign of the charge itself. By the definition of the distribution function it is possible to define a macroscopic field integrating over the velocity coordinate:

$$n_k(\mathbf{x}, t) = \int f_k \mathrm{d}^3 v \tag{2.2}$$

$n_k(\mathbf{x}, t)$ is called particle number density of the kth species. The general moment of the distribution function can be obtained averaging over the velocities:

$$\langle \psi \rangle_k := \frac{\int \psi(\mathbf{v}) f_k \mathrm{d}^3 v}{\int f_k \mathrm{d}^3 v} = \frac{1}{n_k} \int \psi(\mathbf{v}) f_k \mathrm{d}^3 v \tag{2.3}$$

Multiplying eq. 2.1 by ψ and integrating over $\mathbf{v}$ one obtains

$$\int \psi \frac{\partial f_k}{\partial t} \mathrm{d}^3 v + \int \psi \mathbf{v} \cdot \nabla_{\mathbf{r}} f_k \mathrm{d}^3 v + \int \psi \frac{\mathbf{F}_k}{m_k} \cdot \nabla_{\mathbf{v}} f_k \mathrm{d}^3 v = \int \psi C_k \mathrm{d}^3 v \tag{2.4}$$

After some manipulations [28] 2.4 becomes

$$\frac{\partial n_k \langle \psi \rangle_k}{\partial t} + \nabla_{\mathbf{x}} \cdot (n_k \langle \psi \mathbf{v} \rangle_k) - \frac{q_k}{m_k} n_k \left\langle \nabla_{\mathbf{v}} \psi \cdot \left(\mathbf{E} + \mathbf{v} \times \mathbf{B} \right) \right\rangle_k = n_k \langle C_k \psi \rangle_k \tag{2.5}$$

that is an evolution equation for the moment $\langle \psi \rangle_k$. Macroscopic fluid variables can be defined by considering the first few moments of the distribution function.

Taking $\psi(\mathbf{v}) = 1$ in def. 2.3 the number density n_k is recovered as moment of f having as weighting function equal to one. If $\psi(\mathbf{v}) = m_k \mathbf{v}$, then:

$$\langle m_k \mathbf{v} \rangle_k := \frac{1}{n_k} \int m_k \mathbf{v} f_k \mathrm{d}^3 v = m_k \mathbf{u}_k \tag{2.6}$$

where $\mathbf{u}_k$ is the average fluid velocity of the particles belonging to species k^{th}.

The conservation equations for number density and momentum are obtained from eq. 2.5 with some manipulations:

$$\begin{cases} \dfrac{\partial n_k}{\partial t} + \nabla \cdot (n_k \mathbf{u}_k) = S_k \\[2mm] m_k n_k \left[\dfrac{\partial \mathbf{u_k}}{\partial t} + (\mathbf{u_k} \cdot \nabla) \mathbf{u_k} \right] = q_k n_k (\mathbf{E} + \mathbf{u}_k \times \mathbf{B}) - \nabla : \underline{\underline{\mathbf{P_k}}} + \mathbf{R_k} \end{cases} \tag{2.7}$$

with $k = 1 \ldots \mathrm{M}$ and with $\mathbf{R}_k = m_k n_k \langle C_k \mathbf{v} \rangle_k$ the momentum exchange among the kth fluid component and the others species. Typically the most important transfer of momentum

for charged particles is due to collisions with neutrals [21]. The tensor of normal and tangential stresses coming from thermal motion is defined as:

$$\underline{\underline{\mathbf{P_k}}} = p_k \underline{\underline{\mathbf{I}}} + \underline{\underline{\mathbf{\Pi_k}}}$$

More details on the averaging of the Boltzmann equation can be found in ref. [1]. System 2.7 is not closed. The closure that will be provided will specialize the equations for the plasma of interest. Let us consisider each equation separately.

2.1.1.   Continuity equation

In the system 2.7 the continuity equation is:

$$\frac{\partial n_k}{\partial t} + \nabla \cdot (n_k \mathbf{u}_k) = S_k(n) \qquad k = 1 \dots M \tag{2.8}$$

The notation $S_k(n)$ emphasiseas the dependence of S_k on n in general, not only n_k. The term S_k comes from

$$S_k = \int 1 * C_k \mathrm{d}^3 v$$

and expresses the net generation of particles of k type due to ionization and recombination processes, being the contribution coming from Coulomb elastic collision null. Indeed chemical reactions are responsible for a variation in time of the number of particles belonging to a certain species. In the following an entire section is devoted to its definition and from now on, it will be called chemical source term. Another term that appears in this equation is the particle flux:

$$\Gamma_k(\mathbf{x}, t) = n_k \mathbf{u}_k = \int \mathbf{v} f_k \mathrm{d}^3 v \tag{2.9}$$

that will be closed leveraging on the hypotheses that are going to be used to simplify the momentum equation.

2.1.2.   Momentum equation

In the system 2.7 the momentum conservation is expressed by:

$$m_k n_k \left[\frac{\partial \mathbf{u_k}}{\partial t} + (\mathbf{u_k} \cdot \nabla) \mathbf{u_k} \right] = q_k n_k (\mathbf{E} + \mathbf{u}_k \times \mathbf{B}) - \nabla : \underline{\underline{\mathbf{P_k}}} + \mathbf{R}_k \qquad k = 1 \dots M$$

There is no external magnetic field in EHD thrusters so

$$\mathbf{B} = 0$$

Neglecting viscous stresses

$$\underline{\underline{\mathbf{P_k}}} = p_k\underline{\underline{\mathbf{I}}}$$

the momentum transfer due to collisions $\mathbf{R}_k$ can be approximated by a Krook collision operator [21]

$$\mathbf{R}_k = m_k n_k \nu_{m,k} \mathbf{u_k}$$

At atmospheric pressure the collision frequency $\nu_{m,k}$ is such that the material derivative $\frac{d\mathbf{u}_k}{dt}$ can be considered small with respect to the collision term and neglected [8]. Therefore

$$\frac{d\mathbf{u}_k}{dt} = \frac{\partial \mathbf{u_k}}{\partial t} + (\mathbf{u_k} \cdot \nabla)\mathbf{u_k} = 0$$

Finally the momentum equation reads:

$$e\; sign(q_k)\mathbf{E}n_k - \nabla p - m_k n_k \nu_{mk} \mathbf{u_k} = 0 \qquad k = 1\ldots M \tag{2.10}$$

From the kinetic theory, pressure and temperature are related by the Boltzmann constant [15]:

$$p_k = n_k k_B T_k$$

and for an isothermal plasma [21],[8]

$$\nabla p_k = k_B T_k \nabla n_k$$

Considering all these hypotheses, the bulk velocity can be computed as follows:

$$\mathbf{u_k} = \frac{q_k \mathbf{E}}{m_k \nu_{mk}} - \frac{k_B T_k}{m_k \nu_{mk}} \frac{\nabla n_k}{n_k} \tag{2.11}$$

The particle flux is

$$\mathbf{\Gamma}_k = n_k \mathbf{u_k} = \frac{q_k n_k \mathbf{E}}{m_k \nu_{mk}} - \frac{k_B T_k}{m_k \nu_{mk}} \nabla n_k \tag{2.12}$$

$$\mathbf{\Gamma}_k = sign(q_k)\mu_k n_k \mathbf{E} - D_k \nabla n_k \tag{2.13}$$

where

$$\mu_k = \frac{e}{m_k \nu_{mk}}$$

is the mobility coefficient and

$$D_k = \frac{k_B T_k}{m_k \nu_{mk}}$$

is the diffusion coefficient. In this way the Einstein-Smoluchowski relation among the mobility and the diffusion coefficient is recovered:

$$D_k = \frac{k_B T_k}{e} \mu_k \tag{2.14}$$

with

$$V_{th,k} = \frac{k_B T_k}{e}$$

known as the thermal potential. The above computation allows to reduce the complexity of the system 2.7 for the specific case of plasma discharges at atmospheric pressure. Indeed the momentum equation is immediately solved and used to specify the flux in the continuity equation. This way of proceeding is called Drift-Diffusion approximation because of the form of the flux. It is composed of a "drift" term that describes the particles motion due to the electric field and of a "diffusion" term which describe the particles motion due to the density gradients. This term is known as Fick's law, that can be recovered considering the free diffusion case, in which $\mathbf{E} = 0$. In this case the particle flux is:

$$\mathbf{\Gamma}_k = -D_k \nabla n_k \tag{2.15}$$

This derivation is not the most general because of the hypothesis of isothermal plasma. [13] computes the drift-diffusion flux starting from the two-term approximation of the distribution function, without any need of assumptions on the temperature of the plasma. Therefore a more general expression for the flux is:

$$\mathbf{\Gamma}_k = sign(q_k)\mu_k n_k \mathbf{E} - \nabla(D_k n_k) \tag{2.16}$$

with the diffusion coefficient inside the nabla operator. This formulation takes into account the fluxes coming from temperature gradients. However the Fick's law is generally employed in the diffusion part of the particles flux [[2], [10]].

2.1.3.   Chemical source term

After having specified the flux term in the continuity equation, thanks to the drift- diffusion approximation, the source term S_k is explained in the following. The net variation in the number densities is caused by chemical reactions. This section will be devoted to derive ordinary differential equations from a generic chemical reactor.

Given the set of M reactions involving N species

$$\sum_{k=1}^{N} r_{i,k} \, n_k = \sum_{k=1}^{N} p_{i,k} \, n_k \qquad i = 1 \ldots M \tag{2.17}$$

with forward reaction coefficient k_i^f and backward reaction coefficient k_i^b. The rate R_i^f of the ith forward reaction is

$$R_i^f = k_i^f \prod_k n_k^{r_{i,k}}$$

The rate R_i^b of the ith backward reaction is

$$R_i^b = k_i^b \prod_k n_k^{p_{i,k}}$$

The net rate of the ith reaction is

$$R_i = R_i^f - R_i^b$$

Therefore the system of ODEs representing the reactions is

$$S_k = \sum_{i=1}^{M} \left(-R_i^f r_{i,k} + R_i^f p_{i,k} - R_i^b p_{i,k} + R_i^b r_{i,k} \right) = -\sum_{i=1}^{M} R_i \left(r_{i,k} - p_{i,k} \right) \tag{2.18}$$

The Jacobian of S_k is given by

$$\frac{\partial S_k}{\partial n_j} = -(r_{i,k} - p_{i,k}) \frac{\partial R_i}{\partial n_j} \tag{2.19}$$

The reaction coefficients k_i^f and k_i^b have to be modeled. For example the Arrhenius model prescribes the dependency of the reaction coefficients on the temperature

$$k_i^f = A_i^f \exp \left(-\frac{\varepsilon_a}{k_B T_i} \right)$$

where ε_a is the Arrhenius activation energy. A better experimental fitting can be obtained as suggested by [38]:

$$k_i^f = A_i^f T^b \exp \left(-\frac{\varepsilon_a}{k_B T_i} \right)$$

The backward coefficient can be obtained as:

$$k_i^b = k_i^f / K_c(T)$$

where $K_c(T)$ is obtained from the law of mass action:

$$K_c(T) = \frac{\prod_{k=1}^{N} n_k^{p_{i,k}}}{\prod_{k=1}^{N} n_k^{r_{i,k}}}$$

This form of the coefficients is suitable in the problem addressed by this thesis for those reactions that do not involve the electrons. As explained in the section 2.1.4, the local field approximation adopted implies a strong correlation between the local electric field and the electron mean energy. Therefore, the computation of coefficients of those reactions involving electrons is performed thanks to the external software BOLSIG+ [13]. Just as as example the forward coefficients are computed by the following integration :

$$k_i^f = \left(\frac{2e}{m_e}\right)^{\frac{1}{2}} \int_0^\infty \varepsilon \sigma_k F_0 d\varepsilon$$

where ε is the energy in the energy space, σ_k is the cross section and $F_0(\varepsilon)$ is the energy distribution, meaning the energy dependent part of the distribution function f.

There is the possibility of a simplified model for the chemical part of the equations, that indeed is frequently used in discharges simulation, for example in [24]. The idea is to condense the chemical species into ions and electrons, and account for the avalanche ionization process thanks to a coefficient, known as Townsend ionization coefficient α [37]. In this case the rates coefficients would be as computed by [13]

$$R_k = \alpha_k x_k |\Gamma_k|$$

The transport properties of the plasma components need to be specified too. In the drift-diffusion approximation it is of general use the Einstein-Smoluchowski relation between the diffusion coefficient and the mobility depicted in eq. 2.14. In the LFA (see paragraph 2.1.4) the dependence on these coefficients on the temperature is reduced to a dependence on the local electric field.

For the electron population even the transport coefficients are computed though *BOLSIG+*.

Regarding the ions and the neutral species, let hypothesize that the inertial properties of them are equal. In other words, let us consider negligible the mass of the electron lost by

the neutral Argon. This comes to say that:

$$D_{ions} = D_{neutral} = \mu_{ions} V_{th,ions}$$

The ions mobility can be taken from experimental data [26].

2.1.4.   Energy equation

At this point, in the system 2.7 the energy equation is missing. Following the Balcon approach, the gas and the ions temperature is approximated to be constant and equal to the ambient one, therefore their energy equation is not needed under this hypothesis. However in the developed model another hypothesis is added, namely the Local Field Approximation (LFA). The basic assumption is that the only transport mechanism for the electron energy is represented by the collisional processes. Consequently, the fluxes in the electron energy equation can be neglected.

The implication is that the mean electron energy is directly linked to the electric field both spatially and temporally and the energy loss during collisions balances the heating [2]. Therefore all the transport properties, as well as the reaction rate coefficients are dependent on the local electric field. In [2] the LFA assumption was discarded because te electron mean free path of approximately $1\mu m$ is considered not so small with respect to the characteristic distance of field variations in the RF discharges. The discharge simulated in this thesis is a DC one and therefore the only variations in time and space of the field are due to the self consistent field developed by the charged carriers. Therefore the behaviour of the electric field is not known a priori. As a first approximation LFA is considered.

2.1.5.   Electric field

The electric field can be expressed as

$$\mathbf{E} = -\nabla\varphi$$

The electrostatic potential φ satisfies the Poisson equation taking into account the self-consistent effect produced by the charges themselves in the domain:

$$-\text{div}\ (\varepsilon\nabla\varphi) = e\sum_{k=1}^{N} z_k n_k$$

It is useful to introduce the reduced electric field since it is an important parameter for the transport and reactions rate coefficients computation:

$$E_{reduced} = \frac{|\mathbf{E}|}{N}$$

2.1.6. BOLSIG+

Since the external software *BOLSIG+* has been used for computations, it is useful to look at what it does and under which hypotheses. *BOLSIG+* is an user-friendly software that solves the Lorentz Two-Term Approximation (LTTA) for the electron distribution function. The LTTA consists in taking only two terms of the spherical harmonics expansion of the Boltzmann equation written in spherical coordinates in velocity space as in[13], when trying to solve it. Therefore f can be written as

$$f(v, \cos\theta, z, t) = f_0(v, z, t) + f_1(v, z, t)\cos\theta \tag{2.20}$$

where f_0 is the isotropic part of f and f_1 is an anisotropic perturbation; v, θ, z and t are four independent coordinates. Without entering in the details, it is important to know that the LTTA typically fails at very high field values, because of the stronger contribution of f_1. However, when adopted for fluid coefficients calculations, the error is acceptable. Moreover, if the conditions are such that the LTTA is completely inadequate, the entire fluid approach becomes questionable [13].

BOLSIG+ takes as input the cross-sections of the collisions processes the user wants to consider as a function of the energy and other parameters like gas temperature, ionization degree and so on. Tabulated values of the cross-sections for a lot of possible reactions are available at [[27], [40]].

The typical way *BOLSIG+* is used in discharge simulations depends on the fluid model. The Boltzamann solver outputs are tabulated as functions of the local reduced electric field. Therefore if the model lacks an energy equation and LFA is adopted, it is possible to enter in a table with an electric field and linearly interpolate the values. Instead, if the energy equation is added to the model, the coefficients are taken as a function of the mean energy and enter into the table with it. For this thesis a database has been produced in order to have data available for computations in this and future work.

2.2.   Limit of validity of the model

At this point it is important to reason about the limit of validity of the proposed model. First of of all, let us examine the choice of a fluid model. At atmospheric pressure, the high collisionality justifies the assumption of local equilibrium for neutral and heavy ions. The model can be more or less accurate depending on the choice of considering or neglecting an energy equation for these species. At atmospheric pressure, it is relatively safe to consider the neutral gas at ambient temperature. However, if strong electric fields arise they can heat the ions, in addition to the electrons. However, since in this model even the electron temperature is not computed by an energy equation, the level of approximation introduced considering the temperature of the ions constant is much less than the error introduced by the modeling of the electrons. Indeed, the local field approximation was introduced, based on which all the transport properties and rate coefficients related to the electrons are function of the local electric field. The assumption can fail if there are fast spatial and time variations in the field compared to the relaxation time and the mean free path of the electrons. In general, the electrons deserve particular care since they are much lighter than the other components in the gas; the energy from the electric field is firstly transferred to them, and then transmitted to the other components through different processes: dissociation, ionization and excitation, affecting all the transport properties of the plasma [35]. Therefore, it could be relevant to remove the LFA and to compute the electron energy in order to have self consistent chemical kinetics and transport properties. Because of these aspects, the model adopted here can be seen as a first approximation of the discharge. In general the drift-diffusion approximation seems to be good at high pressure[[16][8]]. Finally, the last hypothesis introduced is the adoption of the *BOLSIG+* solver, in particular the LTTA. However, it is coherent with the fluid approach.

Note that the model does not include any radiative transport for the photons. Indeed, it is likely that they are produced and immediately lost. Moreover an onset criterion is not included too, meaning that "ignition" of the corona discharge cannot be seen. As a consequence, it has been considered as that the initial condition is thought to be close to that of a corona discharge that is going towards the self-sustained regime.

2.2.1.   Summary of the equations and boundary conditions

Summarizing, the atmospheric gas discharge in Argon will be modeled by the following equations:

$$\begin{cases} \dfrac{\partial n_k}{\partial t} + \mathrm{div}\,(\mathbf{F}_k) = S_k \qquad k = 1 \dots N \\[2mm] - \mathrm{div}\,(\varepsilon \nabla \varphi) = e \sum_{k=1}^{N} z_k n_k \end{cases} \tag{2.21}$$

with $\mathbf{F}_k$:

$$\mathbf{F}_k = -D_k \nabla n_k + \mu_k\, \mathbf{E}\, sign(q_k) n_k$$

and S_k:

$$S_k = -\sum_{i=1}^{M} R_i\, (r_{i,k} - p_{i,k})$$

Therefore the system is:

$$\begin{cases} \dfrac{\partial n_k}{\partial t} + \mathrm{div}\,(-D_k \nabla n_k + \mu_k\, \mathbf{E}\, sign(q_k) n_k) = -\sum_{i=1}^{M} R_i\, (r_{i,k} - p_{i,k}) \qquad k = 1 \dots N \\[3mm] - \mathrm{div}\,(\varepsilon \nabla \varphi) = e \sum_{k=1}^{N} z_k n_k \end{cases}$$

$$\tag{2.22}$$

with M the number of reactions involved.

Having set $D_k = \mu_k V_{th}$ and $\mathbf{E} = -\nabla\varphi$ and $\gamma_{ik} = (r_{i,k} - p_{i,k})$ the system becomes:

$$\begin{cases} \dfrac{\partial n_k}{\partial t} - \mathrm{div}\left(\mu_k V_{th}\left(\nabla n_k + \nabla\varphi\, \dfrac{sign(q_k) n_k}{V_{th}}\right)\right) = -\sum_{i=1}^{M} R_i \gamma_{ik} \qquad k = 1 \dots N \\[3mm] - \mathrm{div}\,(\varepsilon \nabla \varphi) = e \sum_{k=1}^{N} z_k n_k \end{cases} \tag{2.23}$$

The imposed boundary and initial conditions in a one dimensional domain are:

$$
\begin{cases}
\varphi = 0 & on\ x = 0; \\
\varphi = V_0(t) & on\ x = L \\
\Gamma_e \cdot \hat{n} = 0 & on\ x = 0; \\
\Gamma_e \cdot \hat{n} = n_e \sqrt{\dfrac{k_B T_e}{2\pi m_e}} & on\,x = L; \\
n_{Ar+} = n_{Ar2+} = 0 & on\ x = 0; \\
\Gamma_{Ar+} \cdot \hat{n} = \Gamma_{Ar2+} \cdot \hat{n} = 0 & on\ x = L; \\
\Gamma_{Ar} \cdot \hat{n} = \Gamma_{Ar*} \cdot \hat{n} = 0 & on\ \partial\Omega; \\
n_k(x,0) = n_0(x) & \forall \mathbf{x} \in \Omega
\end{cases}
\tag{2.24}
$$

It is useful now to specify the chemistry of Argon considered in this thesis, taken from [2]. 2.1 shows the complete list of the reactions in the model.

	Reactions	Coefficients	Unit
1	$e + Ar \longrightarrow 2e + Ar^+$	$BOLSIG+$	m^3/s
2	$e + Ar \longrightarrow e + Ar^*$	$BOLSIG+$	m^3/s
3	$e + Ar^* \longrightarrow 2e + Ar^+$	$BOLSIG+$	m^3/s
4	$2Ar^* \longrightarrow e + Ar^+ Ar$	$1.2 \times 10^{-15}(300K/T)^{1/2}$	m^3/s
5	$Ar^+ + 2Ar \longrightarrow Ar_2^+ + Ar$	$2.5 \times 10^{-43}(300K/T)^{3/2}$	m^6/s
6	$e + Ar_2^+ \longrightarrow Ar^* + Ar$	$7 \times 10^{-13}(300K/T_e)^{1/2}$	m^3/s
7	$Ar^* \longrightarrow Ar + h\nu$	5×10^5	m^3/s
8	$e + Ar \longrightarrow e + Ar$	$BOLSIG+$	m^3/s

Table 2.1: Reaction system from Balcon et al.[2]

3 | Mathematical Methods

The model presented in the previous chapter highlights some peculiar features from the mathematical point of view. Understanding the nature of the equations that one wants to solve numerically is fundamental; therefore this chapter aims to present the employed mathematical methods to solve the problem. The weak form of the system 2.23 is derived, and the Continuous Galerkin method is adopted for discrete formulation of the PDEs. The Schafetter-Gummel scheme will be introduced for the flux discretization; the splitting scheme, together with backward differentiation formula and Rosenbrock methods will be adopted for the integration in time.

3.1. Weak formulation

Let's find the week formulation of 2.23.

By multiplying the equations in 2.23 respectively by the test functions $v \in H^1(\Omega)$ and $\omega \in H^1_0(\Omega)$

$$
\begin{cases}
\displaystyle\int_\Omega \frac{\partial n_k}{\partial t} v \mathrm{d}x - \int_\Omega \mathrm{div}\left(\mu_k V_{th} \left(\nabla n_k + sign(q_k)\frac{\nabla\varphi}{V_{th}} n_k \right) \right) v \mathrm{d}x = \int_\Omega S_k(n) v \mathrm{d}x \\[3mm]
\displaystyle- \int_\Omega \mathrm{div}\ (\varepsilon\nabla\varphi)\,\omega \mathrm{d}x = \int_\Omega e \sum_{k=1}^N z_k n_k \omega \mathrm{d}x
\end{cases}
\tag{3.1}
$$

with $k = 1, 2 \ldots N$ Recalling that:

$$
\Gamma_k = \mu_k V_{th} \left(\nabla n_k + sign(q_k)\frac{\nabla\varphi}{V_{th}} n_k \right)
\tag{3.2}
$$

Integrating by parts:

$$
\begin{cases}
\displaystyle\int_\Omega \frac{\partial n_k}{\partial t} v \mathrm{d}x + \int_\Omega \Gamma_k \nabla v \mathrm{d}x - \int_{\partial\Omega} \Gamma_k v \mathrm{d}x = \int_\Omega S_k(n) v \mathrm{d}x \\[3mm]
\displaystyle\int_\Omega \varepsilon\nabla\varphi \cdot \nabla\omega \mathrm{d}x = \int_\Omega e \sum_{k=1}^N z_k n_k \omega \mathrm{d}x
\end{cases}
\tag{3.3}
$$

The only non-null contribution to the weak formulation will come from the Robin conditions imposed on the emitter $(x = L)$ for the electrons. Let's define:

$$a_k(n_k, v) = \int_\Omega \left(\mu_k V_{th} \left(\nabla n_k + sign(q_k) \frac{\nabla \varphi}{V_{th}} n_k \right) \right) \nabla v \mathrm{d}x - \int_{\partial\Omega} \Gamma_k v \mathrm{d}x$$

$$F_k(n, v) = \int_\Omega S_k(n) v \mathrm{d}x$$

$$b(\varphi, \omega) = \int_\Omega \varepsilon \nabla \varphi \cdot \nabla \omega \mathrm{d}x$$

$$c(n, \omega) = -\int_\Omega e \sum_{k=1}^N z_k n_k \omega \mathrm{d}x$$

The weak formulation reads:

$\forall t \in (0, T)$ $Find$ $(n_k, \ \omega) \ \in H_0^1(\Omega) \times H^1(\Omega)$ such that

$$\begin{cases} \varphi(0) = 0 \\ \varphi(L) = V_0 \\ n_{Ar+}(0, t) = n_{Ar2+}(0, t) = 0 \end{cases} \tag{3.4}$$

and that

$$\begin{cases} \int_\Omega \frac{\partial n_k}{\partial t} v \mathrm{d}x + a_k(n_k, v) = F_k(n, v) \qquad \forall k \ and \ \forall(n_k, \ \omega) \ \in H_0^1(\Omega) \times H^1(\Omega) \\ b(\varphi, \omega) + c(n, \omega) = 0 \end{cases} \tag{3.5}$$

3.2. Semi-Discretization via Galerkin Method

Note that the k indicating the kth will be omitted from now on to make the notation lighter. Therefore, the reader should keep in mind that there are as many continuity equations as the number of plasma components considered.

Let us introduce a finite dimensional space $V_h \in H^1(\Omega)$. The semi-discrete Galerkin formulation can be obtained by writing:

$\forall t \in (0, T)$ $Find$ $(n_h, \ \varphi_h) \ \in V_h \times W_h$ such that

$$\begin{cases} \varphi_h(0) = 0 \\ \varphi_h(L) = V_0 \\ n_{Ar+,h}(0, t) = n_{Ar2+,h}(0, t) = 0 \end{cases} \tag{3.6}$$

and that

$$
\begin{cases}
\displaystyle\int_\Omega \frac{\partial n_h}{\partial t} v_h \mathrm{d}v + a(n_h, v_h) = F(n_h, v_h) & \forall k \ and \ \forall (v_h, \omega_h) \in V_h \times W_h \\
b(\varphi_h, \omega_h) + c(n_h, \omega_h) = 0 \\
n_h(\mathbf{x}, 0) = n_{0h}(\mathbf{x}) & in \ \Omega
\end{cases}
\tag{3.7}
$$

where $n_{0,h}$ is the projection of the initial condition into V_h. Next, let us introduce a basis $\{\phi_i\}_{i=1}^{N_h}$ for the space V_h and $\{\psi_i\}_{i=1}^{N_h}$ for the space W_h and expand $n_{k,h}$ and φ_h in term of the basis functions.

$$
n_{k,h}(\mathbf{x}, t) = \sum_{j=1}^{N_h} n_{k,j}(t) \phi_j(\mathbf{x})
\tag{3.8}
$$

$$
\varphi_h(\mathbf{x}, t) = \sum_{j=1}^{N_h} \varphi_j(t) \psi_j(\mathbf{x})
\tag{3.9}
$$

Substituting 3.8 and 3.9 into 3.7 the non linear system assumes a convenient matrix form [29]

$$
\begin{cases}
\mathbf{M}_k \dot{\mathbf{n}}_\mathbf{k} + \mathbf{A}_k \mathbf{n}_\mathbf{k} = \mathbf{M}_k & \forall k \\
\displaystyle\mathbf{P}\varphi = q z_k \mathbf{M_k} \sum_{k=1}^{N} \mathbf{n}_k
\end{cases}
\tag{3.10}
$$

$$
\begin{cases}
\mathbf{M}\dot{\mathbf{n}} + \mathbf{A}\mathbf{n} = \mathbf{f}(\mathbf{n}) \\
\mathbf{P}\varphi - \mathbf{K}\mathbf{n} = 0
\end{cases}
\tag{3.11}
$$

where $\mathbf{n} = \{n_{11} \ldots n_{1N_h}, n_{22} \ldots n_{2N_h}, n_{NN_h} \ldots n_{NN_h}\}^T$ and $\{\varphi_{11} \ldots \varphi_{1N_h}\}^T$. The implemented solver assembles the matrices of 3.11 through the library *bim*[9]. The mass matrix is built using a lumping technique. The right hand side $\mathbf{f}$ is the chemical source term and it obtained by pre-multiplying the chemical rates by the same mass matrix M.

$\mathbf{P}$ is a standard stiffness matrix for a diffusion problem [29].

The library *bim* adopts linear finite elements.

In the next section a brief and heuristic description on how fluxes are discretized is presented.

3.3. Flux discretization

In order to discretize the fluxes in the continuity equation let us introduce a partition τ_h of the 1D interval $[0, L]$. The partition is composed of $N + 1$ elements $K_j = (x_{j-1}, x_j)$ having width $h_j = h = x_j - x_{j-1}$ with $j = 1 \ldots N$.

Considering 3.11, the production of the generic line i of $\mathbf{A}$ by the vector $\mathbf{n}$ will define the discretized flux on the ith element:

$$\Gamma_i = \mathbf{A}_i\mathbf{n} \tag{3.12}$$

Going back in a continuous space, adopting the Scharfetter-Gummel approximation the flux for the kth species is:

$$\Gamma_k = sign(q_k)\mu_k \left(n_k' - n_k\frac{\varphi'}{V_{th_k}} \right) \tag{3.13}$$

With some manipulation [4], the density profile for a negative charge is

$$n(x) = n_0 \left(1 - \frac{x}{L}\right) \frac{B(-\hat{\varphi}')}{B(-\hat{\varphi}'\left(1 - \frac{x}{L}\right))} + n_L \left(\frac{x}{L}\right) \frac{B(\hat{\varphi}')}{B(\hat{\varphi}'\left(\frac{x}{L}\right))} \tag{3.14}$$

with $\hat{\varphi} = \frac{\varphi'}{V_{th_k}}$ and $B(x)$ the Bernoulli function defined as

$$B(x) = \frac{x}{\exp(x) - 1} \tag{3.15}$$

The n_k that have positive charge will have the opposite sign in the argument of the Bernoulli function. The case of neutrals will be discussed in a few lines.

Substituting 3.14 into 3.13 it follows that for a generic k^{th} species:

$$\Gamma_k = sign(q_k)\frac{\mu_k V_{th_k}}{L} \left[n_{k0}B(sign(q_k)\hat{\varphi}') - n_{kL}B(-sign(q_k)\hat{\varphi}')\right] \tag{3.16}$$

This flux for the kth species in the ith interval will be:

$$\Gamma_k, i = sign(q_k)\frac{\mu_k V_{th_k}}{h} \left[n_{kx_{j-1}}B(sign(q_k)\hat{\varphi}') - n_{kx_j}B(-sign(q_k)\hat{\varphi}')\right] \tag{3.17}$$

The case of null gradient in the potential will correspond to pure diffusion. Indeed when

$$\hat{\varphi}' = 0$$

both the Bernoulli weights are equal to one and the flux will be entirely due to the gradient of the density between the two extremes of the interval. This condition allows to describe correctly the particles currents for neutral species. Therefore considering a pure diffusive flux, the fluxes of the neutral plasma components are:

$$\Gamma_{neutral} = \frac{\mu_k V_{th_k}}{h} \left[n_{kx_{j-1}} - n_{kx_j}\right] \tag{3.18}$$

3.4. Time Integration

3.4.1. Splitting

In the conditions studied in this thesis there are different times scales that can be identified. From one side there is the characteristic time of the transport phenomena, on the other side there are the time scales of the chemical reactions.Among the transport processes there is a further time scale separation. Let examine the transport firstly.

The particles, here treated as fluid elements, move because of density gradients in the domain (diffusion) or because they have a non-zero valence number and therefore are subjected to the Coulomb force (drift). Let us consider a situation in which the electric field and the density gradients at a given time are given. Electrons and ions/neutrals show transport time scales very different because of the huge difference in the inertia properties. On average, the electrons are two order of magnitude faster than other components of the plasma, introducing a clear separation of scales.

Even the chemical reactions among themselves show different time scales, with slow and fast reactions, as mentioned when the concept of stiffness was introduced in the previous section. Even comparing the slowest reaction with the fastest particle the separation of scales is clear. Let us make an estimate based on the order of magnitude of the physical property of the problem physical state in the conditions that will be discussed later. Consider an electric field of

$$\mathbf{E} \sim 10^5 \frac{V}{m}$$

and the mobility coefficient for electrons

$$\mu_e \sim 10^{-2} \frac{m^2}{Vs}$$

The electron drift velocity is of order:

$$v_e \sim \mu_e \mathbf{E} \sim 10^3 \frac{m}{s}$$

Regarding the ions consider the mobility

$$\mu_i \sim \times 10^{-4} \frac{m^2}{Vs}$$

Therefore their drift velocity is of order

$$v_e \sim \mu_i \mathbf{E} \sim 10^1 \frac{m}{s}$$

With a length scale of

$$L \sim 10^{-3} m$$

It follows

$$t_{drift,e} \sim 10^{-6}$$

while for ions

$$t_{drift,i} \sim 10^{-4} s$$

where t_{drift} is intended as the time the particle needs to span a length of order L. Let us consider the diffusion process. A simple estimate on the gradient could be

$$\nabla n \sim \frac{n_e}{L} \sim 10^{21} \frac{1}{m^4}$$

The electron temperature could be considered of order

$$T_e \sim 10^4 K$$

There for the thermal potential is

$$V_{th_e} \sim 1 V$$

and the diffusion velocity

$$v_{diff,e} \sim \mu_e V_{th_e} \frac{\nabla n_e}{n_e} \sim 10^1 \frac{m}{s}$$

Finally the diffusion time for electron is

$$t_{diff,e} \sim 10^{-4} s$$

These basic estimates shows how the drift is dominant with respect to diffusion considering for the same plasma components, and that electrons transport is much faster than the ions one, as expected. The drift dominance causes many problems, because it appears as a non linear term in the equations.

Making an estimate of the chemical rates is not so simple because the actual production is related to the density of the plasma components. However, the analysis of the results obtained for the chemical reactions considered in the conditions of interest in chapter 5 show an evolution in time scales of tens of nanoseconds. Even the estimates for the electron drift and diffusion are perfectly compatible with the time required for reaching a stationary solution in the validations test of chapter 4. These aspects make the problem very tough from a mathematical point of view, even in one dimension, making the convergence to a stationary value very slow.

All these considerations on the time scales allow us to introduce the concept of stiffness. "Stiffness" in ordinary differential equations (ODEs) has not a precise definition. It should be considered as a phenomenon that some systems exhibit, rather than a property. However, some pragmatical definitions of stiffness can help in understanding why it is important to be aware if the system one deals with is stiff or not, and how effectively solve it. [14] states: "Stiff equations are problems for which explicit methods don 't work." The same author reports the first opinion on the topic by (Curtiss& Hirschfelder, 1952) that clarifies what is done in the following :"Stiff equations are equations where certain implicit methods, in particular BDF, perform better, usually tremendously better, than explicit ones".[14]

The reason of this behaviour relies on the time scales involved in the problems, with some variables subjected to rapid variations in time and others changing slowly. Another example closely related to this thesis, is offered by the Robertson Problem [31].

$$A \longrightarrow B \qquad c_1^f = 0.04 \tag{3.19}$$

$$2B \longrightarrow B + C \qquad c_2^f = 10^7 \tag{3.20}$$

$$B + C \longrightarrow A + C \qquad c_3^f = 10^4 \tag{3.21}$$
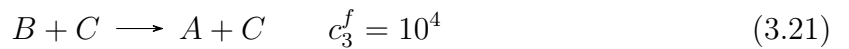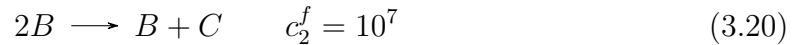
The Robertson problem presents the characteristics of stiff equations, being the time scales of each reaction very different one from the other. This problem is frequently solved to test chemical solvers, therefore also in this work it served as benchmark for the portion of the code devoted to build the chemical source term in chapter 5.

These considerations allow for the adoption of a splitting scheme for the time integration, in which at least the chemical part of eq. 2.8 is solved separately. The discretized problem 3.11 can be written as

$$\mathbf{M}\dot{\mathbf{u}} + \mathbf{L}(\mathbf{u})\mathbf{u} = \mathbf{R}(\mathbf{u}) \tag{3.22}$$

where $\mathbf{u} = \{\mathbf{u}, \varphi\}^T$ in the vector of state variables; $\mathbf{L}(\mathbf{u})$ and $\mathbf{R}(\mathbf{u})$ are the transport and the reaction operator respectively. In a simple splitting scheme the time advancement from t^n to t^{n+1} is realized in two subsequent steps[29].

- First, the reaction operator is applied

$$\mathbf{M}\frac{\tilde{\mathbf{u}} - \mathbf{u}^n}{h^n} = \mathbf{R}(\mathbf{u}^n) \tag{3.23}$$

- In the second step the transport operator is applied

$$\mathbf{M}\frac{\mathbf{u}^{n+1} - \tilde{\mathbf{u}}}{h^n} + \mathbf{L}(\tilde{\mathbf{u}})\tilde{\mathbf{u}} = \mathbf{0} \tag{3.24}$$

with h^n the step size at time t^n.

The splitting operator will introduce an error in the computation, namely the splitting error. However it will make the problem more stable, allowing relatively bigger time steps. Let us analyze each step separately.

3.4.2. Splitting operator: chemistry

In the solver, the integration of 3.23 is done exploiting a backward differentiation formula (BDF) method, in GNU OCTAVE implemented in the function *ode15i* [34].

BDFs are a general class of implicit multi-step methods, among which the most famous is the BDF1, namely Implicit Euler(IE). The accuracy of the solution in IE is closely related to the choice of the step-size, therefore higher order methods are required for bigger h^n.

Equation 3.23 can be written in general terms as follow:

$$My' = f(t, y) \tag{3.25}$$

or fully implicitly as

$$F(t, y, y') = 0; \tag{3.26}$$

The general form of a BDF method with constant step-size is [7]:

$$F\left(t^n, y^n, \frac{1}{\beta_0 h}\sum_{j=0}^{k} \alpha_j y_{n-j}\right) = 0 \tag{3.27}$$

Let examine briefly the way *ode15i* solves these kinds of equations. For simplicity, consider BDF1 that is quite representative of higher order BDF and the notation is lighter ,but with lighter notation.

The 3.27 becomes for a BDF1 method:

$$F\left(t^n, y^n, \frac{y^{n+1} - y^n}{h}\right) = 0 \tag{3.28}$$

At each time step t^n.

The 3.28 is solved by Newton method. In particular the iterate y_m^{n+1} is improved by a

quantity δ

$$y_{m+1}^{n+1} = y_m^{n+1} + \delta$$

δ is found solving the following linear system:

$$F\left(t^n, y_m^n, \frac{y_m^{n+1} - y^n}{h}\right) + \left(\frac{1}{h}F_{y'+F_y}\right)\delta = 0 \tag{3.29}$$

In a higher order BDF the iterative matrix has the form

$$\left(\frac{\alpha}{h}F_{y'+F_y}\right)$$

with α a constant of the method, that will be defined by the order [34]. *ode15i* spans from BDF1 to BDF5.

3.4.3. Splitting operator: transport

The time advancement written in 3.24 is done through a linearly implicit Euler scheme, belonging to the more general family of Rosenbrock methods [14] that were proposed by Rosenbrock [32] in 1963. Again, problem 3.24 can be written in general terms as:

$$My' = f(t, y) \tag{3.30}$$

The implicit Euler is written as:

$$M\frac{y^{n+1} - y^n}{h} = f(t^{n+1}, y^{n+1}) \tag{3.31}$$

The basic idea consists in replacing the Newton iterations that would be required for solving 3.31 with a single one exploiting the derivatives of f [5]. Therefore 3.31 can be written

$$M\frac{y^{n+1} - y^n}{h^n} = f(t^n, y^n) + f_y(t^n, y^n)(y^{n+1} - y^n) \tag{3.32}$$

Rearranging 3.32, it follows

$$(M - h^n f_y(t^n, y^n)) y^{n+1} = My^n + h^n(f(t^n, y^n) - f_y(t^n, y^n)y^n) \tag{3.33}$$

being h^n the step-size at time t^n. The stability properties of this method are the same of Implicit Euler if $f(t, y)$ is a linear function of y, but this is not the case. Therefore stability is a big constraint in the choice of the time step.

This is the reason why the adaptivity of the step-size h^n has been included in the solver.

The user will provide a tolerance *tol* and an estimate of the maximum magnitude of the solution *mag* and then the solver will choose the step-size h^n [30]. As a whole, the solver works as shown in 3.1

Algorithm 3.1 Numerical solution of 3.22

The user provides all the inputs: BCs, initial guess for densitity, coefficients, etc.

for t^n from T^0 to T **do**

    set $u0 = u^n$

    $t^m = t^n$

    while $t^m < t^{n+1}$ **do**

        $t^{m+1} = t^m + h^n$

        Update rate and transport coefficients with $u0$

        Solve the chemistry providing $\tilde{u}$ with $u0$ as initial condition

        Solve the drift-diffusion equation

            compute $v1 = u^{m+\frac{1}{2}}$ using $\tilde{u}$ as initial condition

            compute $v2 = u^{m+1}$ using $v1$ as initial condition

            compute $u1 = u^{m+1}$ using $\tilde{u}$ as initial condition

            compute the error as $err = \frac{v2 - u1}{mag}$

        if $err < tol$ **then**

            $t^m = t^{m+1}$

            increase step-size h^n

            update $u0$ with $u0 = u1$

        else

            $h^n = h^n/2$

        end if

    end while

    Update $u^n = u^{n+1}$

end for

---

4 | Validation of the numerical solver

Since the solver has been written almost from scratch, the majority of the tests that have been performed are for validation purposes, rather than for predictions. Indeed, in the research framework of the IPROP project, different physical features that are not yet modeled are going to be added, as discussed in chapter 6. The tests will validate each part of the solver separately, considering simple cases for which analytical solutions or numerical comparisons are available.

4.1. Test 1: the Robertson Problem

Considering the equation 2.8, the source term is given by the chemical reactions. Therefore, let us consider a generic chemical reactor in the form 2.17. It is required to compute the reaction rates 2.18 and the jacobian of the chemical equations 2.19. As above mentioned, the Robertson problem is frequently used as benchmark in tests. To assess this problem in a general way, it has been implemented an algorithm has been implemented in order to allow the user to provide a *.json* file containing information about reactants, products (with their stoichiometric coefficients) together with the forward and backward rates. For example the input file for the Robertson problem reads:

$$
\{
$$
$$
"reactants" : \{"A" : 1\}
$$
$$
"products" : \{"B" : 1\},
$$
$$
"rate\_coeffs" : \{[0.04, 0]\}
$$
$$
\}
$$
$$
\{
$$
$$
"reactants" : \{"B" : 2\},
$$
$$
"products" : \{"B" : 1, "C" : 1\},
$$
$$
"rate\_coeffs" : \{[3e + 7, 0]\}
$$

}
$\{ \ "reactants" : \{"B" : 1, "C" : 1\}$
$"products" : \{"A" : 1, "C" : 1\},$
$"rate\_coeffs" : \{[1e + 4, 0]\}$
}

This file is read and these informations are used to compute the rates and the Jacobian thanks to two different GNU OCTAVE functions that have been written on purpose. This format can be used whatever the chemical reactor considered. This aspect is quite relevant to make the solver suitable for a broad usage: for example it is possible to simulate the DC discharge in different gas like air or even the same gas but with a different chemistry. The Robertson problem is made of only three species and three reactions, therefore it is simple to compute both the rates and the Jacobian by hand:

$$R_1^f = 0.04 s_A$$

$$R_2^f = 3 \times 10^7 s_B^2$$

$$R_3^f = 10^4 s_B s_C$$

The system of ODEs can be written as:

$$\begin{cases} \dot{s}_A = -R_1^f + R_3^f \\ \dot{s}_B = R_1^f - R_2^f - R_3^f \\ \dot{s}_C = R_2^f \end{cases} \quad (4.1)$$

The Jacobian of this system is:

$$\left[J \right] = \begin{bmatrix} -0.04 & 10^4 s_C & 10^4 s_B \\ 0.04 & -(6 \times 10^7 s_B + 10^4 s_C) & -10^4 s_B \\ 0 & -6 \times 10^7 s_B & 0 \end{bmatrix}$$

For comparison, the Robertson problem has been solved computing rates with the above explained self-coded functions and as suggested by [22]. In both cases, the system of stiff ODEs has been integrated with *ode15i*. The initial conditions are set to be:

$$\begin{cases} A = 1 \\ B = 0 \\ C = 0 \end{cases} \quad (4.2)$$

Results are shown in figure 4.1.
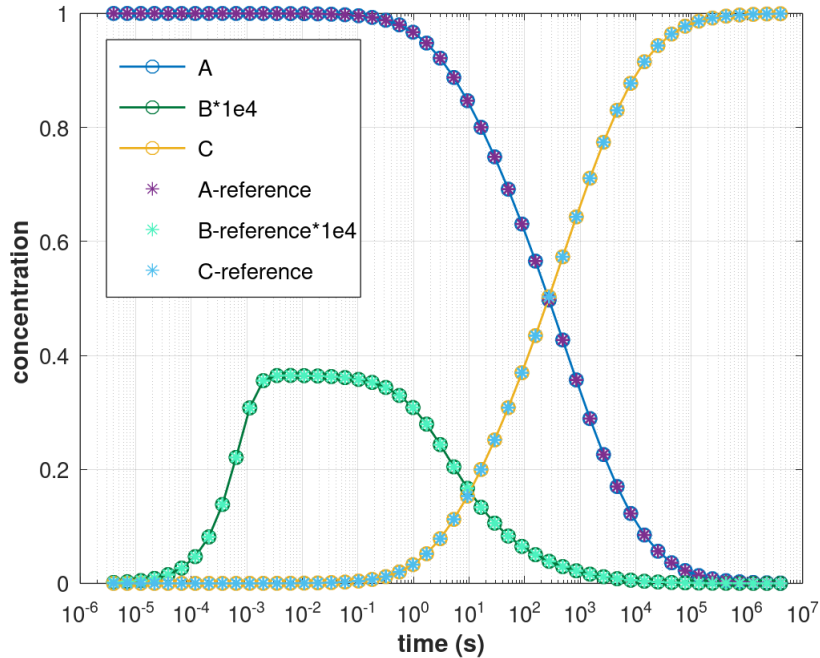
Figure 4.1: Solution of the Robertson problem; reference results from [22]

4.2. Test 2: the Balcon chemical reactor

In this sections some of the results of [36], obtained with *ZDPlasKin* will be correctly reproduced.

Note that, coherently with the hypothesis done in chapter 2 the gas temperature is considered constant in all the computations done by the developed solver. As a consequence, the reaction rate coefficients in which the gas temperature appears are fixed from the beginning. *ZDPlasKin* instead considers, in general, variations in the gas temperature due to collisions. However good agreement is found for relatively low reduced electric field.

The conditions as well as the rates and the results of [36] are given in *cm* rather than in *m*. Only in this section units of measure based on centimeters will be used, just to make the comparison simpler. The initial conditions are set to be:

Parameter	Value	Unit
T_{Ar}	300	K
n_{0Ar}	2.5×10^{19}	cm^{-3}
n_{0e}	1×10^6	cm^{-3}
n_{0Ar^+}	1×10^6	cm^{-3}
n_{0Ar^*}	1×10^3	cm^{-3}
$n_{0Ar_2^+}$	1×10^{10}	cm^{-3}

Table 4.1: Gas temperature and initial conditions

As shown in 2.1 the coefficients for the reactions involving electrons are taken from *BOL-SIG+*. It is possible to exploit the own-built database considering the reduced electric field fixed and changing others parameters like the electron density and the molar fraction of the excited Argon at each time step. Results for $E/N = 1\ Td$ are shown in figure 4.2 and for $E/N = 10\ Td$ in figure 4.3
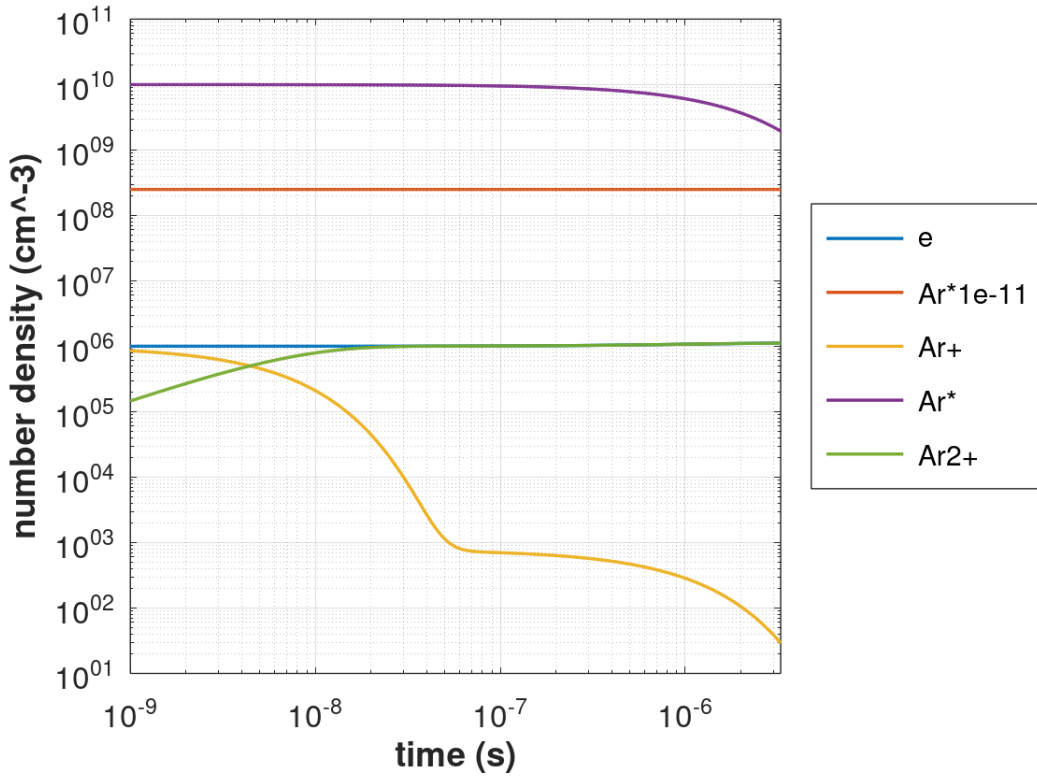
Figure 4.2: Chemical kinetics at $E/N = 1Td$
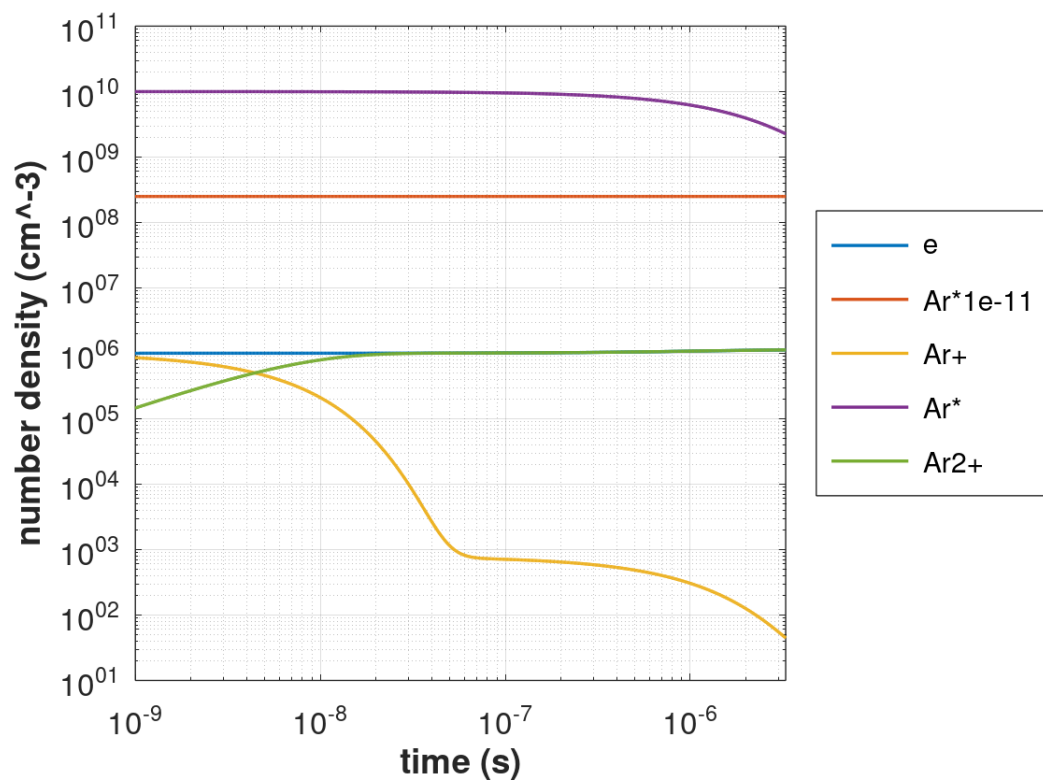
Figure 4.3: Chemical kinetics at $E/N = 10Td$

A more detailed discussion of the Argon kinetics represented can be read in the thesis [36].

4.3.   Test 3: diffusion and Poisson equation

The transport routine of the solver is tested and validated in this section. Let us make some assumptions on the equations 2.23 in order to simplify the system up to the point an analytical solution can be found.

Let us consider only the diffusion contribution of the flux term in the continuity equation:

$$\mathbf{F}_k = -D_k \nabla n_k \tag{4.3}$$

If

$$S_k = 0$$

the system becomes:

$$\begin{cases} \dfrac{\partial n_k}{\partial t} + \text{div}\,(-D_k \nabla n_k) = 0 \qquad k = 1 \dots N & \text{(4.4a)} \\[2mm] -\,\text{div}\,(\varepsilon \nabla \varphi) = e \sum_{k=1}^{N} z_k n_k & \text{(4.4b)} \end{cases}$$

The equation 4.4a is now an heat-like equation and 4.4b is coupled with it in one direction only. Considering the problem in a one dimensional space, it is possible to solve analytically the equation 4.4a and then integrate the Poisson equation to obtain again an analytical expression for the self consistent potential [33]. FOr the sake of simplicity, let consider one species only, for example electrons. The problem to be solved is:

$$\begin{cases} n_t - D n_{xx} = 0 & 0 < x < L;\ 0 < t < T \\ n(x,0) = n_0 & 0 \le x \le L \\ n(0,t) = n_0 & 0 \le t \le T \\ n(L,t) = n_1 & 0 \le t \le T \end{cases} \tag{4.5}$$

with n_0 and n_1 arbitrary constant values, L the dimension of the 1D domain and T the final time considered and $D = \mu_e V_{e,th}$.

The stationary solution is:

$$n^{st}(x, t \to \infty) = \frac{n_1 - n_0}{L} + n_0 \tag{4.6}$$

and the transient is:

$$n^{tr}(x,t) = \sum_{m=1}^{\infty} -\frac{2(n_1 - n_0)}{m\pi}(-1)^m \exp\left(-\frac{m^2\pi^2 D}{L^2}t\right) sin\left(\frac{m\pi}{L}x\right) \tag{4.7}$$

Therefore the complete solution reads:

$$n(x,t) = \frac{n_1 - n_0}{L} + n_0 + \sum_{m=1}^{\infty} \frac{2(n_1 - n_0)}{m\pi}(-1)^m \exp\left(-\frac{m^2\pi^2 D}{L^2}t\right) sin\left(\frac{m\pi}{L}x\right) \tag{4.8}$$

Regarding the potential the solutions is:

$$\varphi(x) = \frac{q}{\varepsilon}\left(\frac{n_1 - n_0}{L}\frac{x^3}{6} + n_0\frac{x^2}{2} - 2Ln_0\right) + \frac{\varphi(L)}{L} + \tag{4.9}$$
$$-\frac{q}{\varepsilon}\sum_{m=1}^{\infty} \frac{2(n_1 - n_0)}{m\pi}(-1)^m \exp\left(\frac{m^2\pi^2 D}{L^2}t\right) sin\left(\frac{m\pi}{L}x\right)$$

A complete derivation of 4.8 can be found in Appendix A.

Table 4.2 resumes the boundary conditions and the transport coefficients that have been adopted for the test. Note that here transport coefficients are given with a reasonable order of magnitude, just for the purpose of the test.

Parameter	Value	Unit
L	2×10^{-3}	m
$n_e(0,t)$	1×10^{18}	m^{-3}
$n_e(L,t)$	1×10^{19}	m^{-3}
$\varphi(0)$	0	V
$\varphi(L)$	500	V
V_{th}	8.63×10^{-1}	V
μ_e	1×10^{-2}	$m^2/(Vs)$
T	2×10^{-4}	s

Table 4.2: Boundary conditions and transport coefficients for test in section 4.3

The results for the computed electron number density compared with the analytical solution 4.8 are shown in figure 4.5 considering three different time instant in order to show both the transient and the stationary solution.

The same is shown for the electric potential in figure 4.6. The relative error for a generic

variable y is:

$$err_{rel} = \frac{\|y_{ex} - y_{computed}\|_\infty}{\|y_{ex}\|_\infty} \tag{4.10}$$

The time history of such defined error, both for φ and n_e, is shown in figure 4.4.
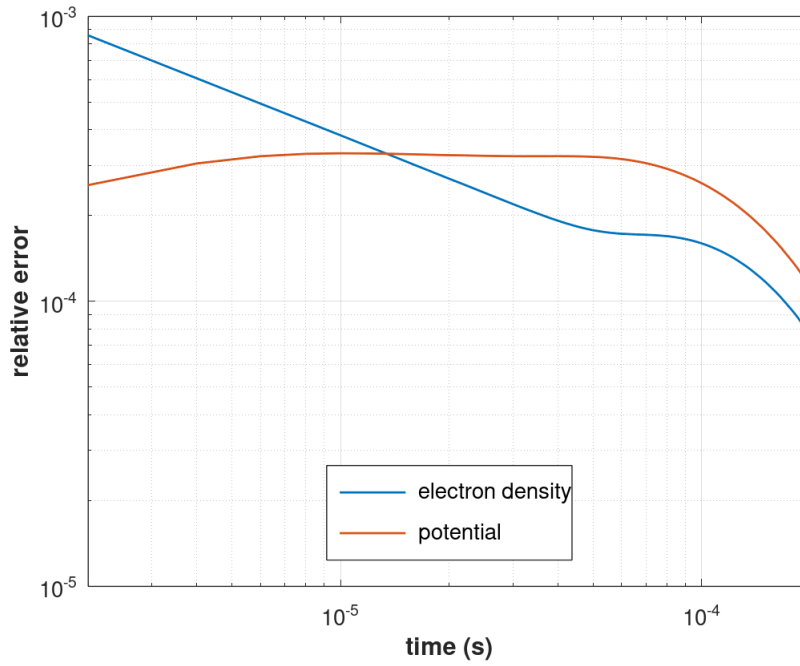
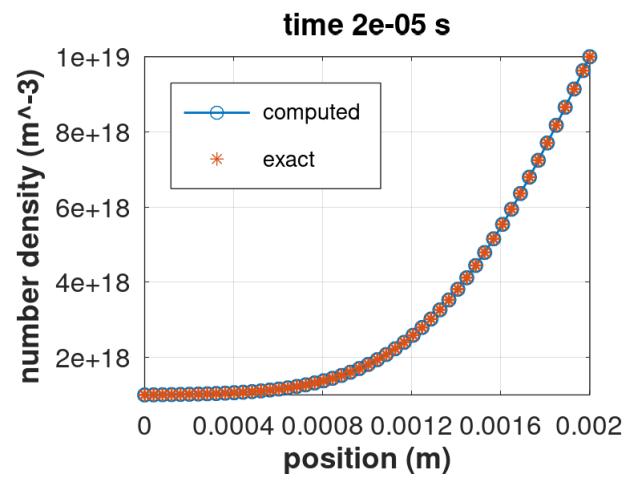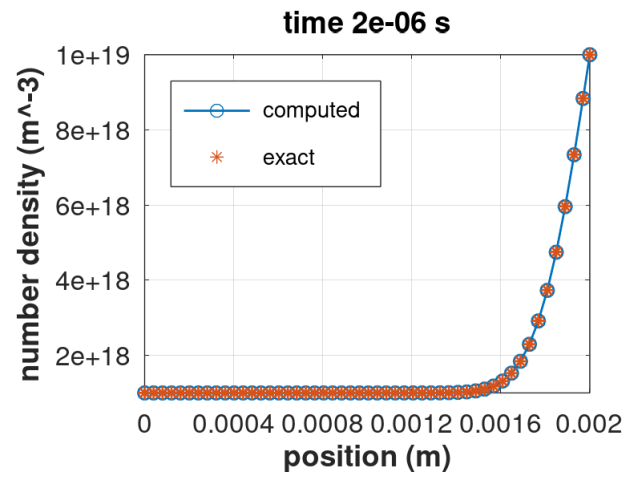Figure 4.4: Relative error computed as 4.10
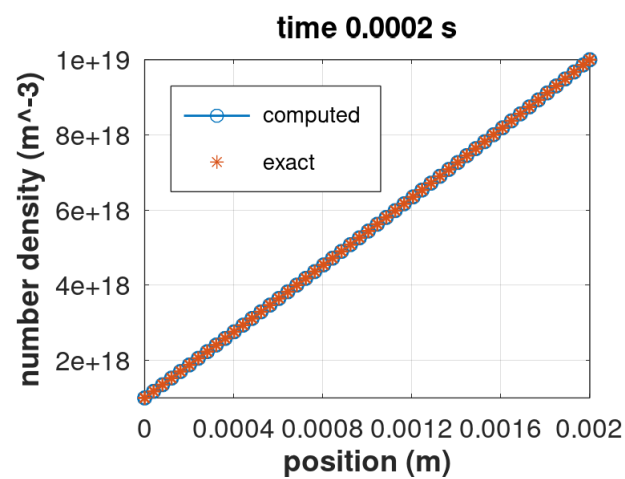
Figure 4.5: Comparison between analytical and computed solution for the electron density at different times
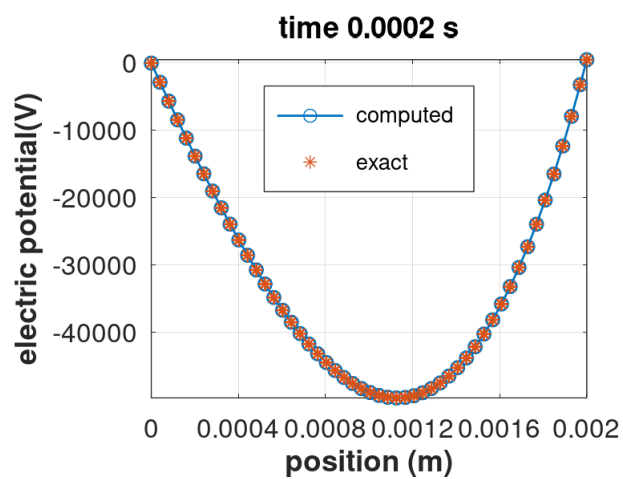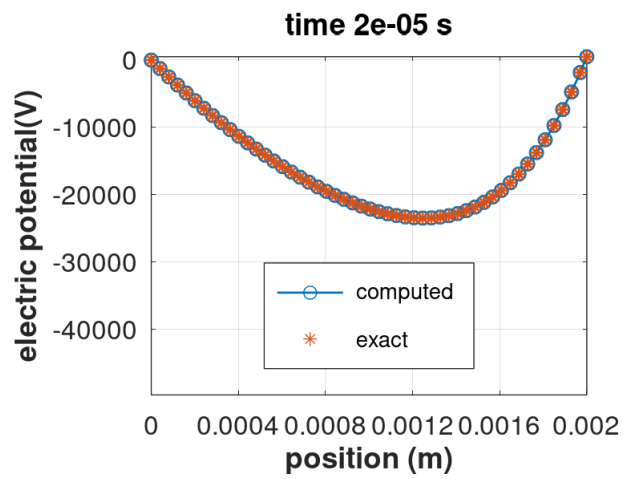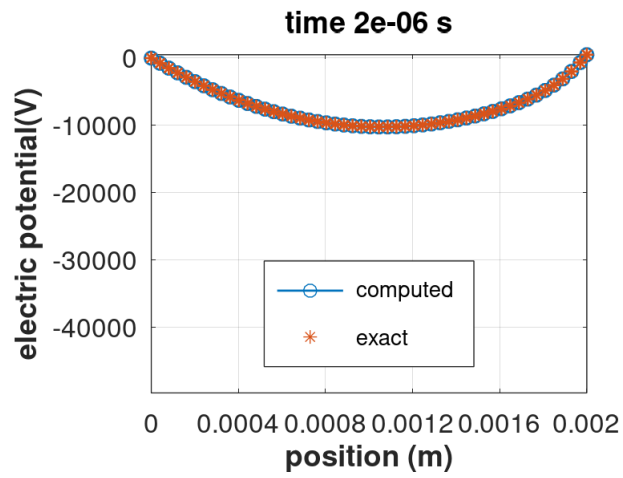
Figure 4.6: Comparison between analytical and computed solution for the electric potential at different times

4.4.   Test 4: drift-diffusion equation

Another that has been performed is related to the drift (and diffusion) part of the solver. In order to be able to find an analytical solution, let us consider again a simpler situation, even if not particularly meaningful from a physical point of view.
Considering only the electrons, the equations are as usual:

$$\begin{cases} \dfrac{\partial n_e}{\partial t} + \text{div}\left(-D_e \nabla n_e - \mu_k \mathbf{E} n_e\right) = 0 & \text{(4.11a)} \\[2ex] -\text{div}\ (\varepsilon \nabla \varphi) = e z_e n_e & \text{(4.11b)} \end{cases}$$

Neglecting the self-consistent effect that electrons have on φ, 4.11b becomes:

$$-\text{div}\ (\varepsilon \nabla \varphi) = 0 \qquad\qquad (4.12)$$

In a one-dimensional domain and with ε constant it is simply:

$$\varepsilon \frac{d^2 \varphi}{dx^2} = 0 \qquad\qquad (4.13)$$

Considering the same boundary conditions

$$\varphi(0) = 0\ V$$
$$\varphi(L) = 500\ V$$

The Poisson equation is immediately solved:

$$\varphi(x) = \frac{V}{L}x \qquad\qquad (4.14)$$

Therefore the electric field is

$$\mathbf{E}(x) = \frac{V}{L}\hat{\mathbf{e}}_x \qquad\qquad (4.15)$$

If the electric field is imposed, the continuity equation can be solved analytically.
Let's look for the stationary solution only, considering the boundary conditions and coefficients reported in table 4.3.

Parameter	Value	Unit
L	2×10^{-3}	m
$n_e(0, t)$	0	m^{-3}
$n_e(L, t)$	4×10^7	m^{-3}
$\varphi(0)$	0	V
$\varphi(L)$	500	V
V_{th}	8.63×10^{-1}	V
μ_e	1×10^{-2}	$m^2/(Vs)$
T	1×10^{-6}	s

Table 4.3: Boundary conditions and transport coefficients for test in section 4.4

$$n_e(0) = 0 \ m^{-3}$$
$$n_e(L) = 4 \times 10^7 \ m^{-3}$$

The stationary solution of 4.11a is

$$n_e(x) = \frac{n_e(L)}{\exp\left(\frac{-|\mathbf{E}|L}{V_{th}}\right) - 1} \left[\exp\left(\frac{-|\mathbf{E}|L}{V_{th}}\right) - 1\right] \tag{4.16}$$

Detailed calculations can be found in Appendix A. The stationary computed solution is then compared with the 4.16 The initial condition set into the solver is

$$n_e(x, 0) = n_e(L)x$$

Comparison between analytical and numerical solution is depicted in figure 4.7
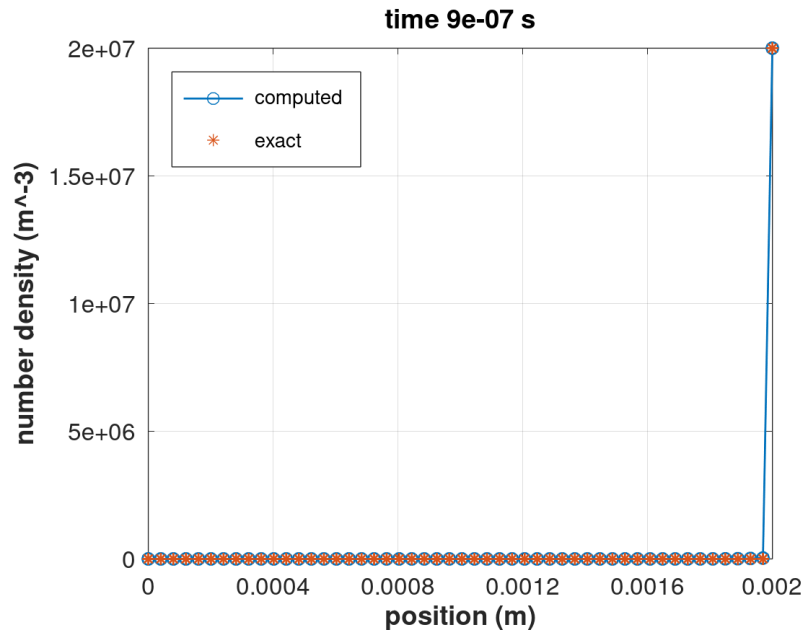
Figure 4.7: 4.16 vs the computed solution

Even if this situation is far from the real conditions of a discharge, some considerations can be drawn. The initial condition is intentionally set such that the gradient in space of the density distribution is opposite to the direction of the electric field. Basically the diffusion would transport the electrons to the left, while the electric field would transport them to the right. The stationary solution clearly shows how the drift component is much stronger than the diffusion term by orders of magnitude. As mentioned, this aspect is an additional complexity from a mathematical point of view because it makes the non linearity of the system stronger.

Furthermore, looking at the time at which the stationary solution is reached in this test and in the previous one in paragraph 4.3, the time scales are comparable with those computed by hand in chapter 3.

For the sake of completeness, the transient solutions at different time instants is shown in fig 4.8.
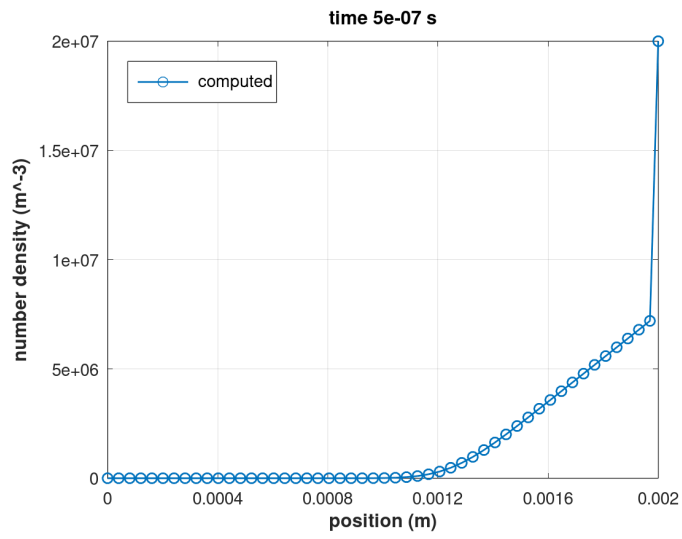
(a)
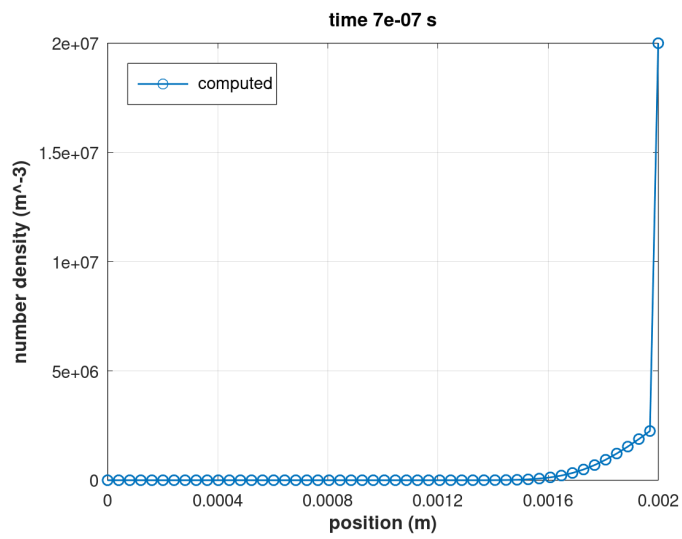
(b)

Figure 4.8: Evolution in time of the electron density under the action of an applied electric field

4.5.   Test 5: drift-diffusion coupled with a simplified chemical source term

The last test is performed considering a problem inherited by the branch of semiconductors for which the solution is known. The equations are basically the same, namely fluid equations in the drift-diffusion approximation and the source term will be a simplified reaction term. Among the validation tests shown in this chapter, this is the only one in which both the chemical and transport part are operating. In the others, being now the chemistry and then the transport turned off, the splitting scheme was not really employed by the solver. The problem solved here is the model of a different physical system. Let's state, at least mathematically, the equations that are going to be solved.

$$
\begin{cases}
\dfrac{\partial n}{\partial t} + \text{div}\,(-D_n\nabla n - \mu_n\,\mathbf{E}\,n) = \dfrac{n_i^2 - pn}{(p+n)\tau} \\[2mm]
\dfrac{\partial p}{\partial t} + \text{div}\,(-D_p\nabla p + \mu_p\,\mathbf{E}\,p) = \dfrac{n_i^2 - pn}{(p+n)\tau} \\[2mm]
-\,\text{div}\,(\varepsilon_r\nabla\varphi) = e(p - n + D - A)
\end{cases}
\tag{4.17}
$$

with n denoting the negative charged carriers and p the positive ones. The boundary conditions for this problem are of Dirichlet type as follows:

$$
\begin{cases}
n(0,t) = p(L,t) = n_i \\
n(L,t) = n(L,0) \\
p(0,t) = p(0,0) \\
\varphi(0,t) = \varphi(L,t) = 0
\end{cases}
\tag{4.18}
$$

with

$$
n_i = 10^{16}\ m^{-3}
$$

and the initial condition is

$$
p(x,0) = \begin{cases}
-\dfrac{D(0)}{2} + \left[\left(\dfrac{D(1)}{2}\right)^2 + n_i^2\right]^{\frac{1}{2}} \exp\left(-\dfrac{1}{10V_{th_p}}\right) & x \le 0.55L \\[4mm]
A(L) + \left[-\dfrac{A(L)}{2} + \left(\dfrac{A(L)}{2}^2 + n_i^2\right)^{\frac{1}{2}}\right] & x > 0.55L
\end{cases}
$$

$$
n(x,0) = \begin{cases}
-\dfrac{D(0)}{2} + \left[\left(\dfrac{D(1)}{2}\right)^2 + n_i^2\right]^{\frac{1}{2}} \exp\left(-\dfrac{1}{10V_{th_n}}\right) & x \le 0.45L \\[4mm]
\left[-\dfrac{A(L)}{2} + \left(\dfrac{A(L)}{2}^2 + n_i^2\right)^{\frac{1}{2}}\right] & x > 0.45L
\end{cases}
$$

A and D are defined as

$$A(x) = \begin{cases} 0 & x \le \frac{1}{2}L \\ a & x \ge \frac{1}{2}L \end{cases}$$

$$D(x) = \begin{cases} a & x \le \frac{1}{2}L \\ 0 & x \ge \frac{1}{2}L \end{cases}$$

The known coefficients are reported in table 4.4

Parameter	Value	Unit
L	1.5×10^{-6}	m
V_{th_p}	2.6×10^{-2}	V
V_{th_n}	2.6×10^{-2}	V
μ_p	0.1	$m^2/(Vs)$
μ_n	0.1	$m^2/(Vs)$
τ	0.1	s
a	1×10^{22}	m^{-3}
ε_r	3.54×10^{13}	$C^2/(Nm^2)$

Table 4.4: Coefficients for the semiconductor problem

The solution is shown in figure 4.9 and 4.10.
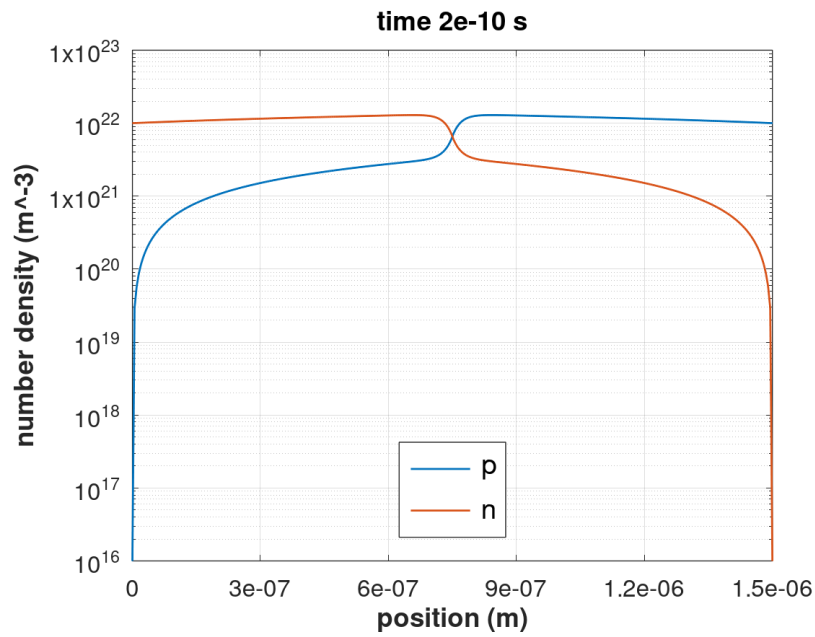
Figure 4.9: p and n number density of 4.17
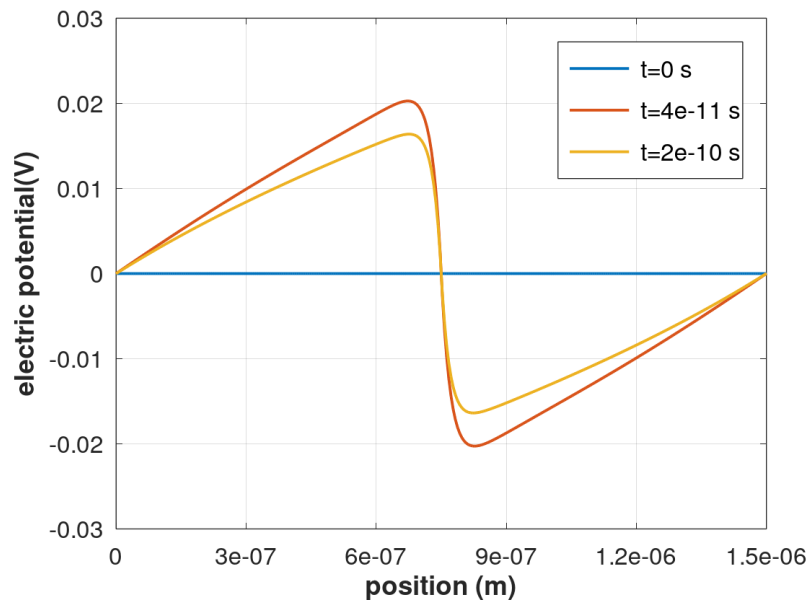
Figure 4.10: Electric potential at different times of 4.17

At this point it has been shown that the solver is capable to simulate all physical phenomena that are included into the model up to now.

5 | Numerical results

In this section, problem 2.23 with boundary conditions 2.24 will be simulated.

As already mentioned in chapter 3 the non linearity of the problem is a source of numerical stability issues. The time step is rigorously chosen by the solver, avoiding the insurgence of numerical instabilities. In order to have a concrete feeling of these problems, some experiments in which the stepsize was arbitrarily chosen by the user from the beginning rather than by the solver have been performed. Even with $h = 1 \times 10^{-9} s$, in few microseconds numerical instabilities set up, preventing convergence.

Reaching a stationary solution employing the very small stepsize chosen by the solver requires very long times making the process unfeasible given the limited time and computational resources available for this work of thesis. Nevertheless, the results that are going to be presented in this chapter, show interesting trends that allow some observations.

As already observed in chapter 2, the model does not include an onset criterion. Therefore the simulation starts from a reasonable initial condition in the form:

$$n_k(x, 0) = A_k \exp\left(-\left(\frac{x-L}{L}\right)^2 A_k\right) \tag{5.1}$$

where A_k will provide the maximum initial density. The neutral Argon instead, is assumed to be constant in the whole domain with an initial density

$$n_{Ar(x,t)} = 2.5 \times 10^{25} \ m^{-3}$$

5.1. Case 1: Constant reaction coefficients

Let consider as a first stage, a condition in which all the reaction and transport coefficients are kept constant, even if this situation is far from the real physics of a discharge. Their initial values will be provided by $BOLSIG+$ in the condition of a reduced electric field of $10 \ Td$. The A_k coefficients for each species are resumed in table 5.1.

Parameter	Value	Unit
A_e	8×10^{17}	m^{-3}
A_{Ar^+}	7×10^{17}	m^{-3}
A_{Ar^*}	1×10^{17}	m^{-3}
$A_{Ar_2^+}$	1×10^{19}	m^{-3}

Table 5.1: Coefficients for the initial density distribution of the plasma components. First simulation.

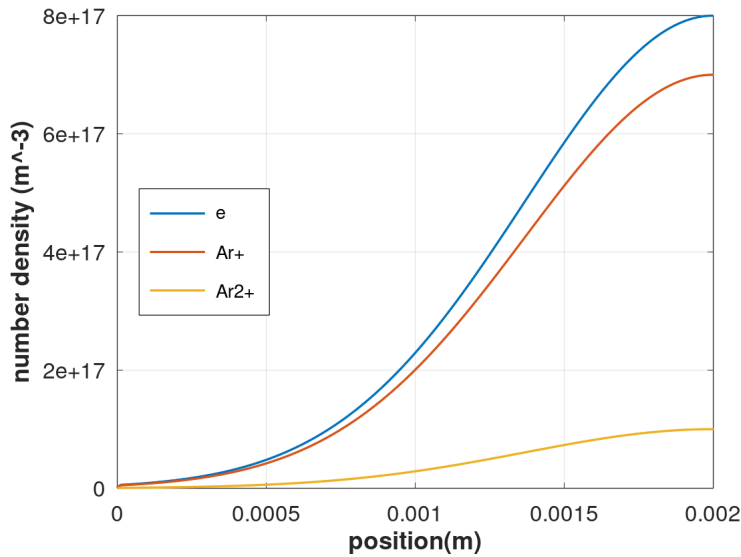The initial condition has been set such to have a globally neutral plasma and it looks like shown in figure 5.1

Figure 5.1: Initial density profiles

The simulation has been performed up to $t = 10^{-6}s$.

In figure 5.2 are shown the time history of the number densities of electrons, ions and excited Argon. On these time scales the chemical term leads the evolution of the density distributions. Indeed, the trend is perfectly coherent with what was observed in paragraph 4.2, even if in different conditions. The discharge appears self-sustained with a clear electron avalanche initiated. The Ar^+ ions show an initial decrease in favours of the dimmers Ar_2^+. This result is coherent with [2], that shows a dominance of ions of molecular Argon at atmospheric pressure.

This aspect, combined with the Neumann condition imposed on the emitter for positive

ions, leads to an increase of Ar_2^+ at the emitter itself. Another observation is related to the confinement of the ion and electron production in the emitter region. 5.2a shows a quite small region near the emitter in which the bulk of the production happens.
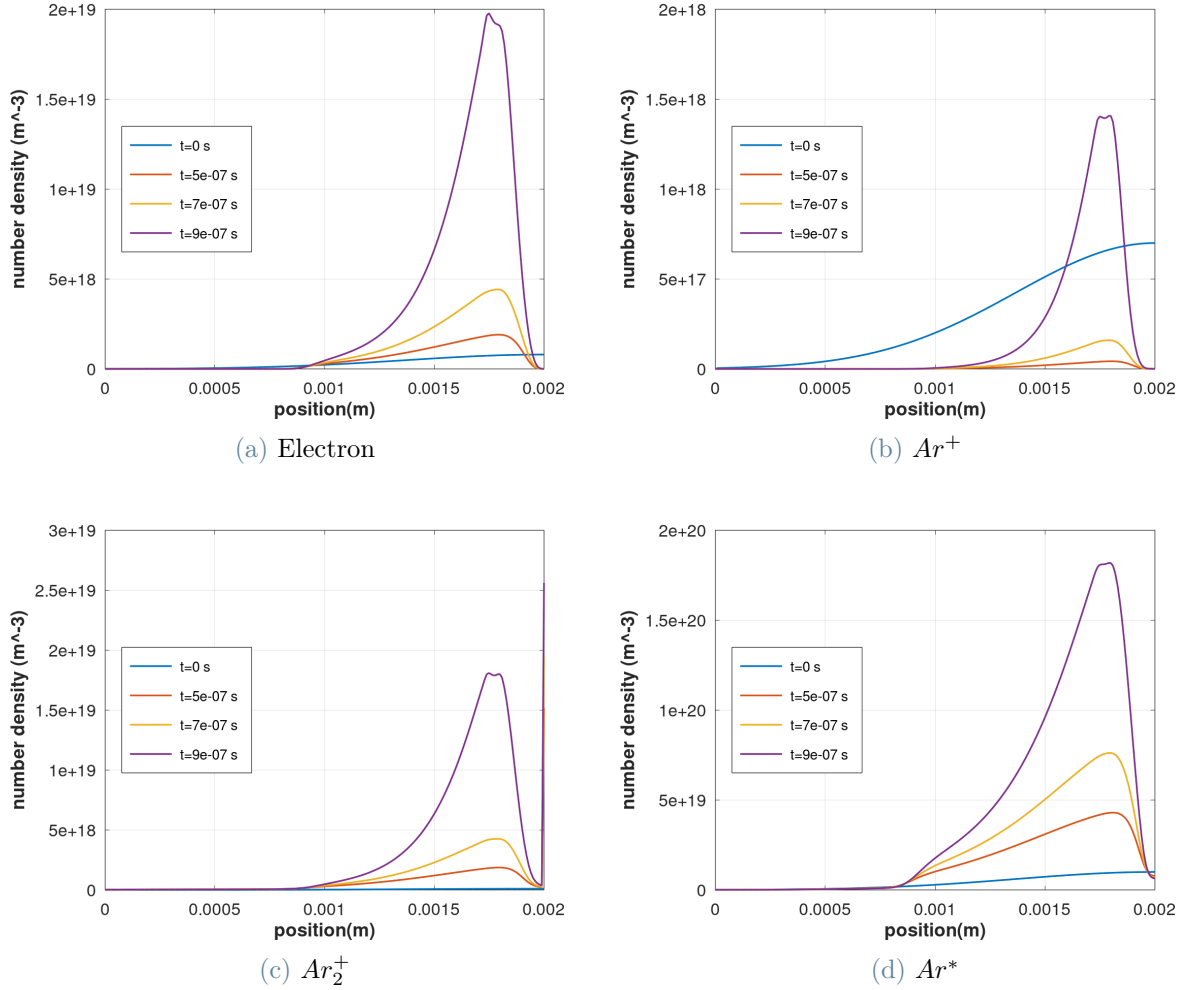

(a) Electron

(b) Ar^+

(c) Ar_2^+

(d) Ar^*

Figure 5.2: Time evolution of the number density of each species

Following the time history of the local densities in one point close to the emitter and collector respectively, this trend is more evident. Figure 5.3a considers $x = 0.1L$ while figure 5.3b consider the point $x = 0.9L$. Ar_2^+ increase relatively slowly, while Ar^+ drop down almost immediately. Therefore the ion current on the collector will be mainly due to the argon dimmers ions. Even electrons drop down quite fast as expected.

On the opposite side, the evolution is clearly towards an increase in time, with the behaviour already depicted for the Ar^+ ions.

(a) Densities in a point near the collector

(b) Densities in a point near the emitter
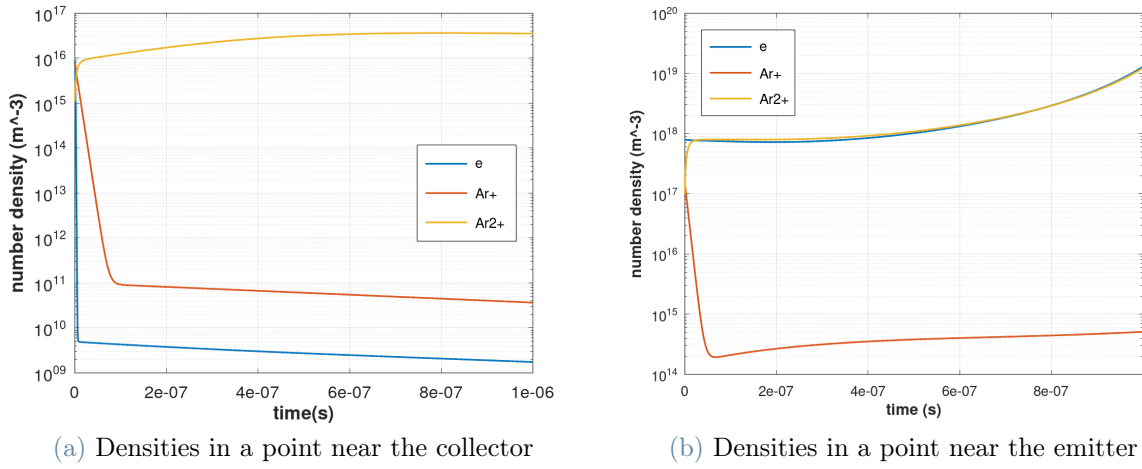
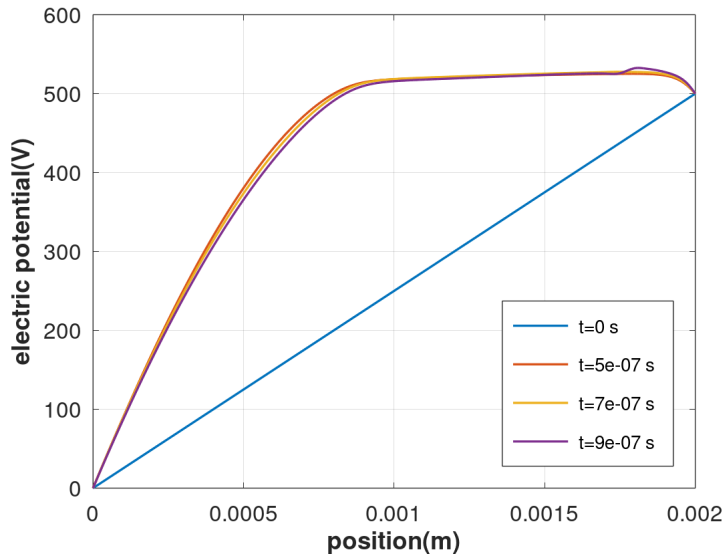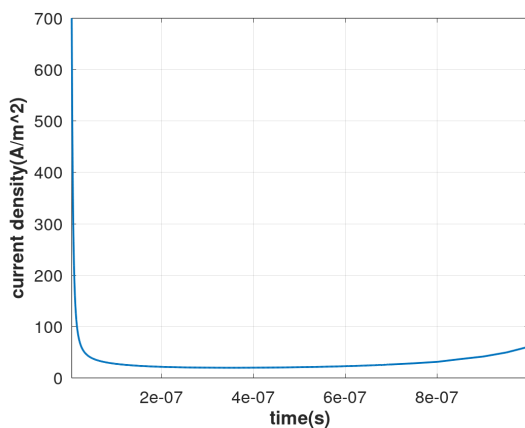Figure 5.3: Time evolution of the densities in specific points

Figure 5.4: Time evolution of the potential

Let us examine what happens in the close vicinity of the emitter. There are few micrometers in which the slope of the potential changes sign, meaning that even the local electric field reverses its sign. As a consequence, some of the electrons locally produced in that region are pushed towards the production region, while ions toward the emitter, adding another reason to the huge number of Ar_2^+ found on the emitter. This phenomenon does not seem to be related to the constancy of the reaction coefficients because it will be there even in the numerical experiment performed in the subsequent paragraph. The question is: where does this phenomenon come from? It can be something related to the LFA

approximation, meaning it fails in that region and the energy equation should be solved. Even the lack of others physical phenomena like ions recombination at the surfaces and secondary emission could be a cause of an error in the densities near the walls. In any case this aspect sets the basis for further investigations to understand if it is a real physical feature or not. If this not a physical effect it is quite relevant the identification of which missing aspect is determinant in the onset of this behaviour.

In the other portion of the domain the potential behaves as expected. The charge production in the production region will create a plateau in the electric potential that shields the emitter from the plasma components that are the far from it. Here the electric field is such that the ions are pushed towards the collector.

Figure 5.5 shows ions and electron current densities of the collector and the emitter respectively. Comparing the electron current density with [2], values are quite similar even in the transient conditions analyzed here.
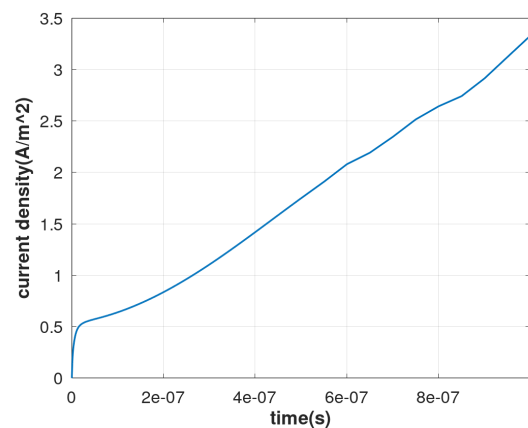
(a) Electron Current Density   (b) Ions current density

Figure 5.5: Time evolution of the current densities

5.2.   Case 2: Variable reaction coefficients

Let us consider the simulation in which the LFA is properly adopted. The qualitative behaviour is not so different from the previous simplified case, but a quantitative analysis shows crucial differences. First of all, given the same initial conditions as before the discharge appears to be not self-sustained. This fact should not be surprising looking the the potential in figure 5.4.

The local field approximation states a strong dependence of the mean electron energies by the local electric field. The solver $BOLSIG+$ computes very low energies when the field goes to zero. This is exactly what happens in the region in which the potential shows a plateau. Therefore more charges are required to start the avalanche process because the reaction coefficients in the production region are lower.

The new A_k coefficients for this simulation are reported in table 5.2

Parameter	Value	Unit
A_e	5×10^{18}	m^{-3}
A_{Ar+}	3×10^{18}	m^{-3}
A_{Ar^*}	2×10^{18}	m^{-3}
$A_{Ar_2^+}$	1×10^{20}	m^{-3}

Table 5.2: Coefficients for the initial density distribution of the plasma components. Second simulation

Moreover it is crucial to have the lowest possible error on the electric field. Otherwise the error in the temperature, that is computed by interpolation entering into the database previously mentioned, is quite high. Oscillations in the field can have serious effect on the electron temperature. This error will propagate on the densities and then again on the field and the temperature. In other words, the same tolerance adopted in the case of constant coefficient will cause a lot of numerical noise on the temperature destroying the quality of the solution. For all these reasons the tolerance has been reduced, making longer the simulation time.

Therefore, in this case a final time of $2 \times 10^{-7}s$ has been reached.

A comparison between initial and final densities is shown in 5.6. As said, the qualitative behaviour is similar: electron and ionized argon dimers show an increment while the $Ar+$ tends to drop down. It is possible to note the same huge increase of Ar_2^+ in the emitter close vicinity, this time with higher values because electron are now hotter there.
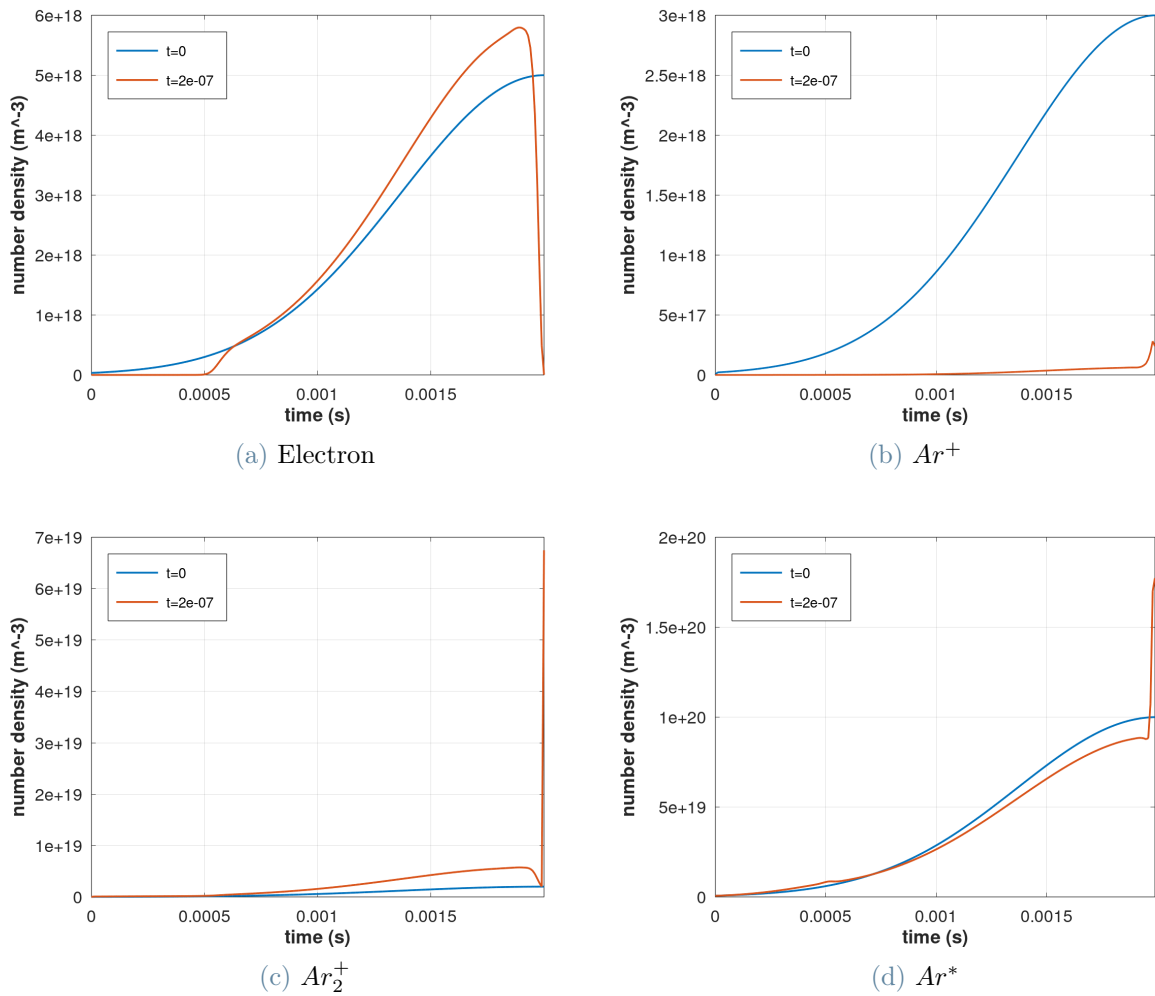
(a) Electron

(b) Ar^+

(c) Ar_2^+

(d) Ar^*

Figure 5.6: Time evolution of the number density of each species with *BOLSIG+* coefficients

The chemical rates are slower than before, because the behaviour of the potential, that is depicted in figure 5.7.
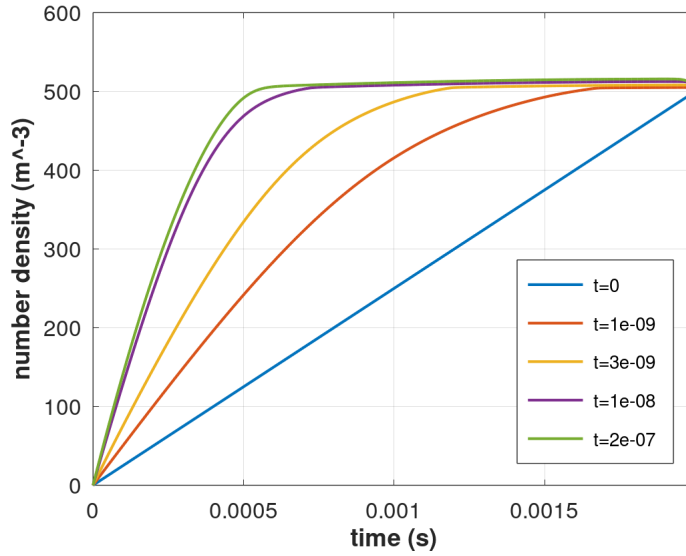
Figure 5.7: Time evolution of the potential

The potential should be observed closely with the temperature, for the reasons explained. The temperature profile evaluated in the same time of 5.7 are shown in figure 5.8.
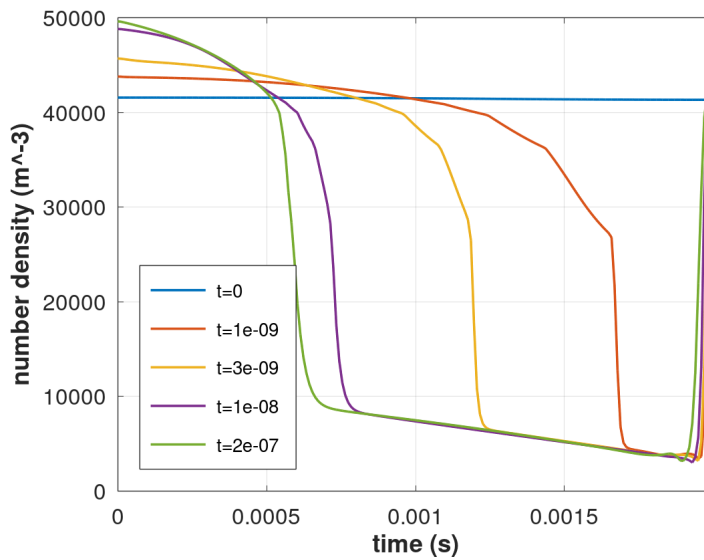

Figure 5.8: Time evolution of the temperature

The rapid increase in temperature experienced near the emitter is perfectly coherent with the computation with *BOLSIG+*.

Further considerations on the extent of the ion production region would be possible letting the simulation go for longer times.

6 | Conclusions

This thesis has been developed within the research plan of the IPROP project and has taken [36] as starting point. This work has been done in parallel with another colleague that focused his attention on the macroscopic flow arising in the discharge [23]. Here the attention has been devoted at proposing a model for microscopic phenomena near the emitter of the EHD thrusters. This model has been analysed, evidencing its main features as well as its limit. Finally the numerical implementation in GNU OCTAVE leads to a solver that, after some validations, allows to look at what happens in a geometry of interest in conditions similar to those of [2].

Some features of the plasma flow are correctly reproduced: the ion generation in a confined production region, the shielding effect that makes flat the potential and a good correspondence between the temperature and the electric field is found as expected without an energy equation. In the following some possible future developments are presented. From a physical perspective the Local Field Approximation (LFA) should be discarded, as pointed out different times, and one should consider an energy equation that allows to be more consistent with the chemical kinetics. Other phenomena like photo ionization and secondary emission will be added. An onset criterion for the discharge would allow to leave behind the problem of the choice of a good initial condition.

Moreover, the Argon gas should be abandoned, in order to work with air since the airships fly in atmosphere and an investigation of which is a good reduced chemical model for air should be carried out. From a numerical point of view the effort should go, on the one hand in the direction of providing numerical stabilization to allow the greatest possible step size, and on the other hand towards the computational efficiency of the solver.

Bibliography

[1] A. I. Akhiezer et al. *Plasma Electrodynamics Vol. 1*. Pergamon Press, 1975.

[2] N. Balcon, G. Hagelaar, and J. Boeuf. Numerical Model of an Argon Atmospheric Pressure RF Discharge. *IEEE Transactions on Plasma Science*, 36(5):2782–2787, 2008.

[3] M. Belan, L. Arosti, R. Polatti, F. Maggi, S. Fiorini, and F. Sottovia. A parametric study of electrodes geometries for atmospheric electrohydrodynamic propulsion. *Journal of Electrostatics*, 113:03043886, 2021.

[4] F. Bosisio. Modelli fisico-matematici per la simulazione numerica di dispositivi a semiconduttore con metodi a volumi misti. Master's thesis, Master Thesis, Politecnico di Milano, 1996.

[5] J. Buthcer. *Numerical Methods for Ordinary Differential Equations*. John Wiley & Sons, Ltd, 2008.

[6] D. Cagnoni. Finite volume electrohydrodynamic simulations of corona discharge in air. Master's thesis, Master Thesis, Politecnico di Milano, 2012.

[7] V. Campbell, S.; Linth and L. Petzold. Differential-algebraic equations. *Scholarpedia*, 3(8):2849, 2008.

[8] F. F. Chen. *Introduction to Plasma Physics and Controlled Fusion*. Plenum Press, New York, 1984.

[9] C. De Falco et al. bim:pde solver using a finite element/finite volume approach, 2014. URL `https://octave.sourceforge.io/bim/overview.html`.

[10] T. Deconinck and L. L. Raja. Modeling of mode transition behavior in argon microhollow cathode discharges. *Plasma Processes and Polymers*, 6(5):335–346, 2009.

[11] S. Fiorini and F. Sottovia. Design and testing of a laboratory setup for ehd propulsion studies. Master's thesis, Master Thesis, Politecnico di Milano, 2019.

[12] A. Fridman, A. Chirokov, and A. Gutsol. Non-thermal atmospheric pressure discharges. *Journal of Physics D: Applied Physics*, 38(2):R1–R24, 2005.

[13] G. J. M. Hagelaar and L. C. Pitchford. Solving the Boltzmann equation to obtain electron transport coefficients and rate coefficients for fluid models. *Plasma Sources Science and Technology*, 14(4):722–733, 2005.

[14] E. Hairer and G. Wanner. *Solving Ordinary Differential Equations II-Stiff and Differential-Algebraic Problems*. Springer-Verlag Berlin Heidelberg GmbH, 1991.

[15] M. Kogan. *Rarefied Gas Dynamics*. Plenum Press, New York, 1969.

[16] V. Kolobov and V. Godyak. Electron kinetics in low-temperature plasmas. *Physics of Plasmas*, 26(6):060601, June 2019.

[17] P. S. Kothnur and L. L. Raja. Two-dimensional simulation of a direct-current microhollow cathode discharge. *Journal of Applied Physics*, 97(4):043305, 2005.

[18] E. Kuffel, W. Zaengl, and J. Kuffel. *High voltage engineering: fundamentals*. Butterworth-Heinemann., 2000.

[19] A. A. Laguna, B. Esteves, A. Bourdon, and P. Chabert. A regularized high-order moment model to capture non-Maxwellian electron energy distribution function effects in partially ionized plasmas. *Physics of Plasmas*, 29(8):083507, 2022.

[20] A. Le, A. Stainer, L. Yin, B. Wethertin, B. Keenan, and B. Albright. Hybrid-vpic: An open-source kinetic/fluid hybrid particle-in-cell code. *Physics of Plasmas*, 30(6), 2023.

[21] M. A. Lieberman and A. J. Litchtenber. *Principles of Plasma discharges and Materials processing*. John Wiley & Sons, Inc, Hoboken, New Jersey, 2005.

[22] MathWorks. ode15i: Solve fully implicit differential equations — variable order method, 2023. URL `https://it.mathworks.com/help/matlab/ref/ode15i.html`.

[23] M. Menessini. Numerical simulations of ion electrodiffusion and advection in atmospheric ionic thrusters. Master's thesis, Master Thesis, Politecnico di Milano, 2023.

[24] N. Monrolin and F. Plouraboué. Multi-scale two-domain numerical modeling of stationary positive DC corona discharge/drift-region coupling. *Journal of Computational Physics*, 443, Oct. 2021.

[25] N. Monrolin, F. Plouraboué, and O. Praud. Electrohydrodynamic thrust for in-atmosphere propulsion. *AIAA Journal*, 55(12):4296–4305, 2017.

[26] N. Nur, N.; Bonifaci and A. Denat. Ionic wind phenomenon and charge carrier mobility in very high density argon corona discharge plasma. *Journal of Physics: Conference Series*, 495:012041, 1952.

[27] L. Pitchford et al. Lxcat: an open-access, web-based platform for data needed for modeling low temperature plasmas. *Plasma Processes and Polymers*, 14(1-2): 1600098, 2016.

[28] G. Pucella and S. E. Segre. *Fisica dei Plasmi*. Zanichelli, 2009.

[29] A. Quarteroni. *Modellistica numerica per problemi differenziali*. Springer, 2008.

[30] F. Quarteroni, A.;Saleri and G. P. *Calcolo Scientifico: Esercizi e problemi risolti con MATLAB e Octave*. Springer Milan, 2017.

[31] H. Robertson. *The solution of a set of reaction rate equations. Numerical Analysis, an Introduction*. Academic Press, 1966.

[32] H. H. Rosenbrock. Some general implicit process for the numerical solution of differential equations. *The Computer Journal*, 5(4):329–330, 1963.

[33] S. Sandro. *Equazioni a derivate parziali*. Springer Milan, 2016.

[34] L. F. Shampine. Solving $0 = f(t, y(t), y'(t))$ in matlab. *Journal of Numerical Mathematics*, 10(4):291–310, 2002.

[35] F. Taccogna and G. Dilecce. Non-equilibrium in low-temperature plasmas. *The European Physical Journal D*, 70(11):251–288, 2016.

[36] N. Tamburini. Simulazioni numeriche di plasmi non termici mediante modelli globali. Master's thesis, Thesis, Alma Mater Studiorum-Universitá di Bologna, 2021.

[37] J. Townsend and P. Edmunds. Lxxxix. the discharge of electricity from cylinders and points. *The London, Edinburgh, and Dublin Philosophical Magazine and Journal of Science*, 27(161):789–801, 1914.

[38] W. Vicenti and C. Kruger Jr. *Introduction to Physical Gas Dynamics*. Robert E. Krieger Publishing CO., Inc., 1965.

[39] H. Xu, Y. He, K. L. Strobel, C. K. Gilmore, S. P. Kelley, C. C. Hennick, T. Sebastian, M. R. Woolston, and S. R. H. Perreault, D. J.and Barrett. Flight of an aeroplane with solid-state propulsion. *Nature*, 563:532–535, 2018.

[40] S. Yamabe, C.; Buckman and A. V. Phelps. Measurement of free-free emission from low-energy-electron collisions with ar. *Physical Review A*, 27(3):1345–1352, 1983.

A | Appendix A

A.1. Analytical solution of the heat-like equation for the diffusion problem

Let consider the following partial differential equation:

$$\begin{cases} n_t - Dn_{xx} = 0 & 0 < x < L; \, 0 < t < T \\ n(x,0) = n_0 & 0 \leq x \leq L \\ n(0,t) = n_0 & 0 \leq t \leq T \\ n(L,t) = n_1 & 0 \leq t \leq T \end{cases} \tag{A.1}$$

First of all the stationary solution can be found integrating two times

$$n_{xx} = 0$$

obtaining

$$n(x) = Ax + B$$

with A and B to be determined by the boundary conditions. It is easy to compute

$$A = \frac{n_1 - n_0}{L}$$

and

$$B = n_0$$

The transient solution is defined as

$$n^{tr}(x,t) = n(x, t \to \infty) - n(x,t) = \frac{n_1 - n_0}{L}x + n_0 - n(x,t)$$

The transient solution satisfies the original equation with different conditions:

$$
\begin{cases}
n^{tr}(x,0) = 0 & 0 \leq x \leq L \\
n^{tr}(0,t) = 0 & 0 \leq t \leq T \\
n^{tr}(L,t) = \dfrac{(n_1 - n_0)}{L}x & 0 \leq t \leq T
\end{cases}
\tag{A.2}
$$

Employing the separation of variables:

$$
n^{tr} = \omega(x)v(t)
\tag{A.3}
$$

Substituting into the equation in A.1 follows

$$
v_t \omega - D v \omega_{xx} = 0
$$

that can be written as

$$
\frac{v_t}{v} = D\frac{\omega_{xx}}{\omega} = \lambda
$$

where λ is a constant to be determined. Consider the equation for ω

$$
\begin{cases}
\omega_{xx} - \dfrac{\lambda}{D}\omega = 0 & 0 \leq x \leq L \\
\omega(0) = \omega(L) = 0
\end{cases}
\tag{A.4}
$$

with $\frac{\lambda}{D} = -\mu^2 < 0$. The solution is in the form

$$
\omega(x) = A\sin\mu x + B\cos\mu x
$$

Leveraging on the boundary conditions, it follows that

$$
\begin{cases}
\omega_m = a\sin\mu x \\
\mu = \dfrac{m\pi}{L} & m = 1,2\ldots\infty \\
\lambda = -\mu^2 D
\end{cases}
\tag{A.5}
$$

The equation for v is

$$
v = \lambda v
$$

and therefore

$$
v(t) = \exp(\lambda t) = \exp\left(-\frac{m^2\pi^2}{L^2}Dt\right)
$$

Summing up all the ω_m and substituting into A.3 the candidate solution reads

$$n^{tr}(x,t) = \sum_{m=1}^{\infty} A_m \exp\left(-\frac{m^2\pi^2 D}{L^2}t\right) sin\left(\frac{m\pi}{L}x\right) \qquad (A.6)$$

A_m can be found considering expanding the initial condition for n^{tr} in Fourier series

$$\frac{n_1 - n_0}{L}x \simeq \sum_{m=1}^{\infty} A_m \sin(\frac{m\pi}{L}x)$$

$$A_m = \frac{2}{L}\int_0^L \frac{n_1 - n_0}{L}x\sin(\frac{m\pi}{L}x)dx = -\frac{2(n_1 - n_0)}{m\pi}(-1)^m$$

The solution A.6 to now is only a candidate one. [33] demonstrates that A.6 is the right solution and that is unique. Finally n reads

$$n(x,t) = \frac{n_1 - n_0}{L} + n_0 + \sum_{m=1}^{\infty}\frac{2(n_1 - n_0)}{m\pi}(-1)^m \exp\left(-\frac{m^2\pi^2 D}{L^2}t\right) sin\left(\frac{m\pi}{L}x\right) \qquad (A.7)$$

The Poisson equation in 1D is

$$\frac{d^2\varphi}{dx^2} = \frac{e}{\varepsilon}n$$

Therefore the first integration leads to

$$\varphi(x) = \frac{e}{\varepsilon}\left(\frac{n_1 - n_0}{L}\frac{x^3}{6} + n_0\frac{x^2}{2} - 2Ln_0\right) + \frac{\varphi(L)}{L} + \qquad (A.8)$$
$$-\frac{e}{\varepsilon}\sum_{m=1}^{\infty}\frac{2(n_1 - n_0)}{m\pi}(-1)^m \exp\left(\frac{m^2\pi^2 D}{L^2}t\right) cos\left(\frac{m\pi}{L}x\right)$$

and finally the potential is

$$\varphi(x) = \frac{e}{\varepsilon}\left(\frac{n_1 - n_0}{L}\frac{x^3}{6} + n_0\frac{x^2}{2} - 2Ln_0\right) + \frac{\varphi(L)}{L} + \qquad (A.9)$$
$$-\frac{e}{\varepsilon}\sum_{m=1}^{\infty}\frac{2(n_1 - n_0)}{m\pi}(-1)^m \exp\left(\frac{m^2\pi^2 D}{L^2}t\right) sin\left(\frac{m\pi}{L}x\right)$$

with the stationary values that read:

$$\varphi(x,t\to\infty) = \frac{e}{\varepsilon}\left(\frac{n_1 - n_0}{L}\frac{x^3}{6} + n_0\frac{x^2}{2} - 2Ln_0\right) + \frac{\varphi(L)}{L} \qquad (A.10)$$

A.2.   Analytical solution of the stationary continuity equation when a constant field is applied

Let consider again the continuity equation for the electrons:

$$\frac{\partial n_e}{\partial t} + \text{div}\left(-D_e \nabla n_e + \mu_e \, \mathbf{E} \, sign(q_e)n_e\right) = 0 \tag{A.11}$$

Consider the electric field constant:

$$\mathbf{E}(x) = \frac{V}{L}\hat{\mathbf{e}}_x \tag{A.12}$$

Looking for stationary solution in 1D the eq. A.11 becomes:

$$\frac{d}{dx}\left(-D_e\frac{dn_e}{dx} - \mu_e \, En_e\right) = 0 \tag{A.13}$$

with E the magnitude of the field with its sign. Considering the transport coefficients constant and since even the filed is independent from the x variable, it follows

$$-D_e\frac{d^2 n_e}{dx^2} - \mu_e \, E\frac{dn_e}{dx} = 0 \tag{A.14}$$

This is a second-order ordinary differential equations with constant coefficients Let's rewrite eq. A.14 as follows:

$$\frac{d^2 n_e}{dx^2} + a\frac{dn_e}{dx} = 0 \tag{A.15}$$

with

$$a = \frac{\mu_e E}{D_e}$$

The characteristic polynomial is

$$P(\lambda) = \lambda^2 + a\lambda$$

with two real and different zeros:

$$\lambda_1 = 0$$

$$\lambda_2 = -a$$

The solution is in the form:

$$n_e(x) = C_1 \exp\left(\lambda_1 x\right) + C_2 \exp\left(\lambda_2 x\right)$$

Therefore

$$n_e(x) = C_1 + C_2 \exp{(\lambda_2 x)}$$

Applying the boundary conditions

$$n_e(0) = 0 \ m^{-3}$$

$$n_e(L) = 4 \times 10^7 \ m^{-3}$$

It follows that the solution of A.14 is:

$$n_e(x) = \frac{n_e(L)}{\exp{\left(\frac{-|\mathbf{E}|L}{V_{th}}\right)} - 1} \left[\exp{\left(\frac{-|\mathbf{E}|L}{V_{th}}\right)} - 1\right] \tag{A.16}$$

List of Figures

List of Tables

List of Symbols

Variable	Description	SI unit
f_k	distribution function in phase space of the kth species	$m^{-6}s^{-3}$
n_k	number density of the kth species	m^{-3}
D_k	diffusion coefficient of the kth species	m^2/s
Vth_k	thermal potential of the kth species	V
μ_k	electrical mobility of the kth species	V
q_k	charge of of the kth species	C
e	elementary charge	C
k_B	Boltzmann constant	JK^{-1}
ε	vacuum dielectric constant	$CV^{-1}m^{-1}$
Γ_k	flux of the kth species	$m^{-2}s^{-1}$
S_k	chemical source term in the kth continuity equation	$m^{-3}s^{-1}$
$\mathbf{E}$	electric field	Vm^{-1}
φ	self-consistent electric potential	V
k^f	forward rate coefficient	m^3s^{-1}
k^b	backward rate coefficient	m^3s^{-1}
R^f	forward reaction rate	$m^{-3}s^{-1}$
R^b	forward reaction rate	$m^{-3}s^{-1}$
α	Townsend ionization coefficient	m^{-1}
V	voltage applied on the emitter	V

Ringraziamenti

Ringrazio i miei relatori prof. Paolo Barbante, prof Carlo De Falco e prof Lorenzo Valdettaro, per i preziosi consigli e per avermi messo nelle condizioni di potermi dedicare a una sfida scientifica entusiasmante.

Ringrazio i miei genitori per avermi permesso di studiare lontano da casa con i sacrifici che ne conseguono. Ringrazio mia sorella Federica, per aver saputo crescere anche quando ero lontano e mia sorella Maria Chiara per avermi raggiunto a Milano per i suoi studi; i miei nonni e le mie zie per essersi presi cura di me anche a distanza non facendomi mancare mai nulla.

Ringrazio Sara, che è entrata nella mia vita nel momento in cui ho iniziato questa tesi, per aver reso più dolce questo periodo e aver saputo avere pazienza nei momenti più difficili.